
Article:
O'Brien, C.T., Virtanen, T., Donets, S. et al. (10 more authors) (2021) Control of the aqueous solubility of cellulose by hydroxyl group substitution and its effect on processing. Polymer, 223. 123681. ISSN 0032-3861

https://doi.org/10.1016/j.polymer.2021.123681

Control of the aqueous solubility of cellulose by hydroxyl group substitution and its effect on processing

Cate T. O'Brien[a], Tommi Virtanen[b], Sergii Donets[c], James Jennings[a], Olga Guskova[c], Anna H. Morrell[a], Matt Rymaruk[a], Leena Ruusuvirta[d], Juha Salmela[d], Harri Setala[b], Jens-Uwe Sommer[c], Anthony J. Ryan[a] and Oleksandr O. Mykhaylyk[a]*

[a]Department of Chemistry, Dainton Building, University of Sheffield, Brook Hill, Sheffield, South Yorkshire, S3 7HF, UK

[b]VTT Technical Research Centre, Tekniikantie 4E, FI-02044 VTT, Espoo, Finland

[c]Institute Theory of Polymers, Leibniz-Institute of Polymer Research, Dresden, Hohe Str. 6, 01069, Dresden, Germany

[d]Spinnova, Palokärjentie 2-4, 40320, Jyväskylä, Finland

*corresponding author: o.mykhaylyk@sheffield.ac.uk

Keywords: cellulose, modification, birefringence, rheology, spinning, small-angle X-ray scattering (SAXS), Molecular dynamics simulations

Abstract

Native cellulose is insoluble in water, despite the high number of hydrogen bonding sites per chain, as molecules preferably hydrogen bond to each other, preventing its use in industrial applications. The modification of cellulose has received considerable recent attention, motivated by the move away from conventional petroleum-based, water-soluble polymers, however, a systematic analysis of the effects of modification is rare. Herein a detailed study of hydroxypropyl (HP)- and (2-hydroxypropyl) trimethylammonium chloride-modified cellulose, with degrees of substitution (DS) determined by NMR, establishes modification-property relationships. TEM, small-angle X-ray scattering and rheology demonstrated that increasing DS gradually changes the aqueous solubility, resulting in the formation of different morphologies, including micron-sized aggregates, needle-like cellulose nanoparticles (CNPs) and solvated molecules. It was found that aqueous dispersions with DS_{HP} of 50 %, assigned to a 'sweet spot' in cellulose modification, are suitable for the fiber formation. It is shown that this state of the material can be easily detected by rheo-optical methods based on birefringence. Using structural analysis, molecular dynamic simulation and fiber-spinning results, it is proposed that co-existing CNPs and cellulose molecules, interacting via H-bonding, form a network which orients under shear, acting as a precursor for the fiber formation from aqueous solutions.

TOC

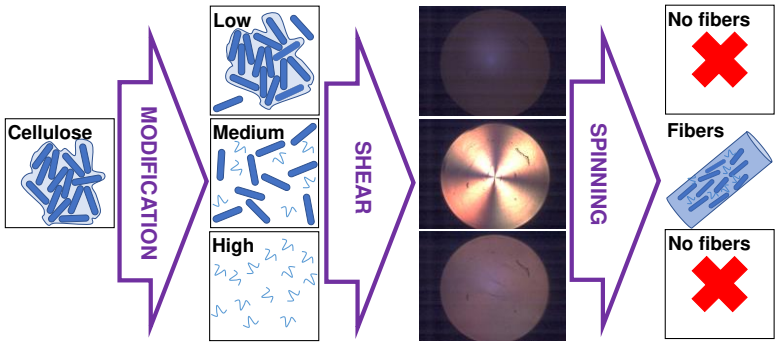
Cellulose
MODIFICATION
Low
Medium
High
SHEAR
SPINNING
No fibers
Fibers
No fibers

1. Introduction

Cellulose is an abundant, naturally occurring polymer found in algae [1,2], bacteria [1–5] and green plants [1,2,6,7] where it exists in a semi-crystalline state [8–12]. The monomer unit consists of two pyranose (a six-membered ring consisting of five carbon atoms and one oxygen atom) rings, with each ring containing one hydroxymethyl group and two hydroxyl groups (Figure 1) [13]. The presence of such functional groups leads to many hydrogen bonding sites along the polymer chain [14]. This extensive hydrogen bonding produces a stiff chain [15], enabling its use in plant cell walls where it acts as a scaffold [11,16]. Surprisingly, despite the high number of hydrogen bonding sites per chain, cellulose is insoluble in water and most organic solvents [14], as the cellulose molecules hydrogen bond to each other, rather than with solvent molecules [17].

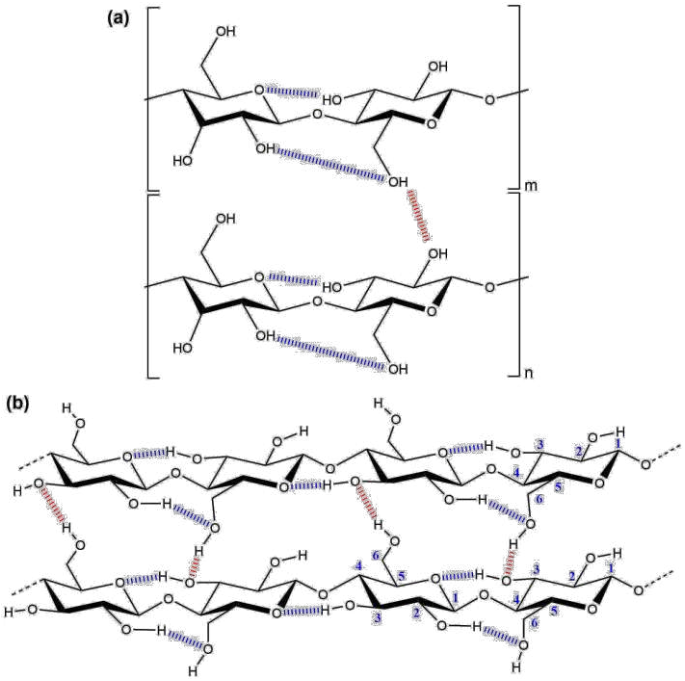

Figure 1. (a) Cellulose repeat unit structure, depicting the glycosidic linkages between the carbon rings, intramolecular hydrogen bonds (blue dashed lines) and intermolecular hydrogen bonds (red dashed lines) [2,18,19]; n and m indicated the degree of polymerization of the adjacent molecules. **(b)** Extended cellulose structure depicting intra- and intermolecular hydrogen bonds and the numbering system of carbons in a pyranose ring indicated by the blue numbers (1 – 6).

The inherent stiffness of the molecules as well as the extensive hydrogen bonding leads to the formation of highly oriented structural domains, causing cellulose to be birefringent [20]. Birefringence occurs when a material exhibits more than one refractive index, with each depending on the polarization and propagation of incident light. The degree of birefringence observed in cellulosic materials is directly related to the amount of lateral order within a fiber [20]. Due to this property, birefringence measurements have been utilized extensively in the research of these materials [17,21–24]. For example, birefringence has been used to demonstrate the alignment of individual crystal nanofibers in cellulose. Work performed independently by Mendoza-Galvan *et al*. and Hamza *et al*. investigated the degree of orientation in fibers during, or after, being stretched [24,25]. Both observed birefringence caused by the presence of long-range order of cellulose molecules within the fiber. The manifestation of birefringence in cellulose films has led to research into the application of cellulose in optical displays, such as liquid crystal displays (LCDs) [26].

Despite cellulose being frequently utilized in its native form in the paper and textile industries [27,28], a lack of water solubility prevents it being used more widely in most industrial applications. There is a number of approaches used to process cellulose to make it suitable for various applications: chemical modifications producing processable cellulose derivatives soluble in water and many organic solvents, or grinding/fibrillation/fluidization of cellulose into nanocellulose. Chemical modification to alter the cellulose structure has proven to be particularly effective [29,30]. Consequently, the modification of cellulose has received considerable attention over the last 150 years [13], from both industry and academia, with a recent wave of interest motivated by the move away from traditional petroleum-based polymers [1,2,5,31]. Of the different modification strategies utilized, the most

common target functionalization is the hydroxyl groups present on the cyclic backbone [11,32–34].

By performing selective modification of these hydroxyl groups, a range of properties can be introduced or altered depending on the substitution groups being used. In particular, solubility and viscosity of cellulose derivatives such as hydroxypropyl (HP) or hydroxypropylmethyl, or cationized (cat) cellulose are dependent on the degree of molar substitution (MS), distribution and type of substituents, and molecular weight of cellulose and cellulose derivatives. For example, when MS_{cat} of the cationized β-1,3-glucan [35] or cellulose of cotton linter pulp [36] is higher than 0.16 or 0.2, respectively, the cationized celluloses are water-soluble. Whereas, Schaller *et al*. have shown that 2,3-*O*-hydroxypropyl cellulose prepared regioselectively in heterogeneous reaction conditions already soluble in water when MS_{HP} is 0.8 [37]. Moreover, Gosecki *et al.* prepared hydroxypropyl celluloses with various degree of substitutions and further modified them to produce methyl carbamate derivatives [38]. The solubility behavior and cloud point of the hydroxypropyl cellulose methyl carbamates in water solution were clearly dependent on the degree of substitution and molar masses of the cellulose derivatives. According to Bochek, the higher the degree of substitution of the hydroxyl groups, the lower the solubility parameter of cellulose acetate starting from 55.7 $J^{-1/2}$ $cm^{-3/2}$ for unmodified cellulose [39]. The Hildebrand solubility parameter provides an estimation for the degree of interaction between materials; a solute and solvent with similar solubility parameters are likely to be miscible [40]. Furthermore, when the solubility parameter is equal to or lower than that of water (23.5 $J^{-1/2}$ $cm^{-3/2}$), dissolution of cellulose occurs [39]. This work highlights the ability to tailor the properties of cellulosic samples by simple modification routes to produce desirable

effects. However, cellulose molecular weight could be an important factor to consider as well. It has been demonstrated that the choice of cellulose with relatively low molecular weight (< 100 kDa) is essential for both the ease of dissolution and structural properties of spun fibres such as degree of orientation and crystallinity [41]. Thus, high molecular weight cellulose, with an increased number of entanglements between molecular chains, is neither good for dissolution nor fiber mechanical properties. Another property of cellulose that can be altered through modification is the gelation behavior of cellulose solutions; Gallego *et al.* found that the gel strength, of cellulose modified with isocyanates, was dependent on the amount of non-polar groups present after modification [42].

In theory, the material properties of cellulose can be tuned for a desired application by selectively controlling both the degree of modification and the chemical nature of the modifying groups. However, a systematic analysis of the effect of the extent and type of modification on the bulk properties of modified cellulose, involving experimental and theoretical techniques, is rare. In this study, cellulose was originally modified with HP groups in order to improve cellulose solubility in water and then with a cationic component to facilitate processability of the derived material. A wide range of characterisation techniques were used in this work to study the effect of the chemical modification on the water solubility of cellulose, structural morphologies, birefringence and the rheological behavior, with a view to produce products suitable for fiber formation and to provide guidelines for characterization of cellulose derivatives. In addition, molecular dynamic simulations are used to investigate the effect of modification on cellulose with a direct focus on water solubility and structural properties. As an auxiliary technique, the

thermodynamic integration for evaluation of the Helmholtz hydration free energy to quantify each modification made to the native monomeric unit of cellulose is utilized.

2. Experimental

2.1. Materials

Spruce cellulose powder was used for modification reactions [22183-1KG-F, Sigma Aldrich, Missouri, USA; weight-average and number-average molecular weights of M_w = 92 kDa and M_n = 18.5 kDa, respectively, both determined by size exclusion chromatography using 2 x PL gel MiniMixed A columns with a precolumn in DMAc/0.8% LiCl eluent (0.36 ml/min, T = 80 °C) and a Waters 2414 Refractive index detector]. The cellulose molar mass distribution was calculated against eight pullulan standards (6.1 kDa ≤ M_n ≤ 70.8 kDa) using Waters Empower 3 software[43]. Propylene oxide (PO) (> 99.5 w/w %), (2-hydroxypropyl)trimethylammonium chloride (HPTMAC) (> 90 w/w % and 2-4 w/w % of chlorohydrin impurities) used as a 70 w/w % aqueous solution, *tert*-butanol (*t*-BuOH) (> 99.5 w/w %) used as 90 w/w % aqueous solution (water was added before usage), NaOH (50 w/w % solution in H_2O), NaOD [40 w/w % solution in D_2O (99 atom % D)] were all purchased from Sigma Aldrich (Missouri, USA). 10 v/v % sulfuric acid and 3.7 v/v % hydrochloric acid freshly prepared from 98 v/v % sulfuric acid and 37 v/v % hydrochloric acid, respectively were used for neutralizations.

2.2. Chemical Modification

Four different cellulose derivatives with various degrees of molar hydroxyl substitution by HP per anhydroglucose unit (AGU) were prepared and coded to be $C_{7/0}$ (MS_{HP} = 0.21), $C_{27/0}$ (MS_{HP} = 0.8), $C_{50/0}$ (MS_{HP} = 1.5) and $C_{80/0}$ (MS_{HP} = 2.4). These samples had a corresponding percentage degree of substitution by HP (DS_{HP}) of 7%, 27 %, 50 %, and 80 %, respectively [Table 1 and Figure 2, step (i)]. They were synthesized according to the following procedure: 100 g of cellulose powder (0.617 mol of AGUs) was suspended in the mixture of 150 ml of 10 M NaOH (diluted from 50 w/w % NaOH), 450 ml of water, and 300 ml of 90 w/w % aqueous *t*-BuOH.

The mixture was stirred overnight at 30 °C. 216 (3.09 mol), 430 (6.14 mol) or 648 (9.26 mol) ml of PO was then added slowly to the mixture in three portions (a single addition taking about 15-20 min) with 2-3 h intervals between additions during one working day followed by stirring overnight at 30 °C. The reaction mixture was cooled down to 20 °C and neutralized with 10 v/v % sulfuric acid until a pH of 7 – 8 was reached. The reaction mixture was then dialyzed using a 3500 MWCO membrane (Thermo Fisher Scientific, Massachusetts, USA) and freeze-dried.

$C_{27/0}$ and $C_{50/0}$ were further used as starting materials for cationization [Figure 2, step (ii)]. The molar ratio of HPTMAC/AGU was either 2.59 or 7.91 for cationization targets with MS_{cat} of 0.24 (DS_{cat} = 8 %) or 0.75 (DS_{cat} = 25 %), respectively. The degrees of hydroxypropylation and cationization represented as the percentage of substituents on the cellulose are used for sample labelling (Table 1). For example, $C_{50/8}$ was prepared from 20 g of $C_{50/0}$ (0.081 mol, calculated from the average molecular weight of one $C_{50/0}$ AGU, which is 247.86 g/mol) suspended in 180 ml of water. 14.6 g of 50 w/w % NaOH (0.183 mol) was added to adjust the molarity to 0.88 M (in the reaction mixture after HPTMAC addition). The reaction mixture was then heated up to 45 °C and 45.2 g of 70 w/w % HPTMAC water solution (0.209 mol of HPTMAC) was then added slowly during 10-15 min to reach the HPTMAC/AGU molar ratio of 2.59. The mixture was stirred overnight at 45 °C. The reaction mixture was cooled down to 20 °C and neutralized with the hydrochloric solution to pH 7-8. The reaction mixture was dialyzed using a 3500 MWCO membrane and then freeze-dried to a white powder.

$C_{7/25}$ was synthesized as follows; 30 g (0.185 mol of AGU) of cellulose powder (Fluka 22182) was suspended in a mixture of water (70 ml), tBuOH (200 ml), and NaOH (7.1 g, 50 w/w % NaOH solution). The mixture was stirred overnight at 25 °C

before 50 ml (0.71 mol) of PO was added slowly and stirred for 4 h at 25 °C. The mixture was then heated to 45 °C. 177 ml (0.923 mol, 70 w/w % solution) of HPTMAC was added slowly and the mixture was stirred overnight. The reaction mixture was cooled to 20 °C and neutralized with conc. HCl to pH 7-8. The reaction mixture was dialysed using a membrane with 3500 cut-off and then freeze-dried to a white powder. Prior to their use, all modified cellulose samples were dispersed at required concentrations in deionized water by gentle mixing overnight.

2.3. Determination of solid content by centrifugation measurements

The insoluble solids content of the modified cellulose was analyzed for a 5 w/w % solution by centrifuging each sample for 1 h at 5000 rpm. The sediment and solution parts were divided, and the sedimented part was washed once with deionized water before being centrifuged again. The sediments thus obtained were dried in an oven at 110 °C for 2 h before being weighed and the sediment dry mass content was calculated.

2.4. ^{1}H and ^{13}C nuclear magnetic resonance (NMR)

Chemically modified cellulose powders were characterized using solid-state ^{13}C NMR spectroscopy (see Supplementary data, Figure S1). The solid-state cross-polarization (CP) magic angle spinning (MAS) ^{13}C NMR measurements were performed with an Agilent 600 DD2 NMR spectrometer with a magnetic flux density of 14.1 T. The spectra were recorded at 22 °C using a triple resonance probehead operating at double resonance mode, with MAS rate of 10 kHz. For each spectrum 8000 scans were recorded with a 6 s delay between the scans. The contact time for cross polarization was 1.3 ms. Protons were decoupled during acquisition using SPINAL-64 proton decoupling with a field strength of 80 kHz. Pulse durations and Hartmann-Hahn match were calibrated using α-glycine. The spectra were processed

using Bruker TopSpin 3.6 software. The DS was determined by comparing the integrals originating from HP and HPTMAC and the C1 signal of cellulose with the aid of signal deconvolution (Figure S1). Since the CP/MAS method emphasizes ^{13}C nuclei close to protons, it is not a quantitative method, and only gives an estimate of the total degree of substitution for comparison purposes. The solid state CP/MAS ^{13}C NMR was used as a semi-qualitative method to prove the success of syntheses.

^{1}H NMR spectra were recorded for a 5 w/w % sample in D_2O using a 400 mHz Avance III HD 400 spectrometer (Bruker, Massachusetts, USA) equipped with a double resonance broadband optimized probehead. The experiment was performed with 16 scans averaged per spectrum.

2.5. Elemental analysis

C, H, N, S and O contents were determined using a FLASH 2000 series analyzer (Thermo Fisher Scientific, Massachusetts, USA). A modified cellulosic sample was weighed in tin capsules before being placed inside a MAS 2004 auto-sampler (Thermo Fisher Scientific, Massachusetts, USA) at a pre-set time and then dropped into an oxidation/reduction reactor kept at 900 – 1000 °C. The amount of oxygen required for optimum combustion was delivered into the reactor at a precise time. The reaction of oxygen with the tin capsule at elevated temperatures generates an exothermic reaction which raises the temperature to 1800 °C. At this temperature, both organic and inorganic substances are converted into elemental gases which, after further reduction, are separated into a chromatographic column and detected by a highly sensitive thermal conductivity detector. The determination of oxygen is performed via pyrolysis in the same analyzer. The detection limit of the method is 0.1 w/w %. Results were calculated using certified elemental microanalysis standards

using K factor and the CHNS/CHNS-O Standards Kit (Elemental Microanalysis, Devon, UK).

2.6. Zeta potential measurements

The measurements were performed using a Malvern Zetasizer Nano ZS (Malvern Panalytical, Malvern, UK) instrument. 0.1 w/w % aqueous dispersions of modified cellulose prepared from the whole sample were analyzed at 25 °C in the presence of 1 mM KCl. Zeta potentials were calculated from the Henry equation using the Smoluchowski approximation [44]. All data were averaged over ten consecutive runs.

2.7. Transmission electron microscopy (TEM)

Imaging was performed using an Technai Spirit 2 microscope (FEI, Oregon, USA) operating at 80 kV and fitted with an Orius SC1000B camera (Gatan, California, USA). Copper/palladium TEM grids (Agar Scientific, UK), coated in-house with a thin film of amorphous carbon and subsequently subjected to a glow discharge for 20 s, were used as sample holders. Individual 10 µL droplets of 0.1 w/w % aqueous dispersions (without removal of insoluble material) of modified cellulose were placed on freshly treated grids for 1 minute and then blotted with filter paper to remove excess solution. To ensure sufficient contrast, uranyl formate (10.0 µL of a 0.75 w/w % solution) was absorbed onto the sample-loaded grid for 30 s and then blotted to remove any excess of the stain compound. Each freshly loaded grid was then dried under vacuum conditions. Size of the particles observed in TEM images was analyzed using ImageJ software [45]. The average particle size for each image was calculated from 25 independent measurements.

2.8. X-ray scattering measurements

Small-angle and wide-angle X-ray scattering patterns (SAXS/WAXS) were collected using a laboratory SAXS/WAXS beamline (Xeuss 2.0, Xenocs, Grenoble, France) equipped with a liquid gallium MetalJet X-ray source (Excillum, Kista, Sweden, X-ray wavelength λ = 0.134 nm), FOX3D single reflection multi-layered X-ray mirror and two sets of motorized scatterless slits for beam collimation, a Pilatus 1M pixel SAXS and a Pilatus 100k pixel WAXS detectors (Dectris, Barden-Daetwil, Switzerland). SAXS patterns were recorded over a range of 0.03 $nm^{-1} < q < 1.3$ nm^{-1}, where $q = (4\pi\sin\theta)/\lambda$ is the scattering vector length and θ is one-half of the scattering angle. SAXS/WAXS patterns of modified cellulose aqueous dispersions (without removal of insoluble material) diluted to 1 w/w % concentrations were recorded using glass capillaries of 2 mm diameter (WJM-Glas, Berlin, Germany) as a sample holder. X-ray scattering data reduction (calibration and integration) was performed using the Foxtrot software package supplied with the instrument and further data analysis (background subtraction and data modelling) was carried out using Irena SAS macro [46] for Igor Pro software package.

2.9. Rotational rheology and shear-induced polarized light imaging (SIPLI)

The measurements were performed using a stress-controlled MCR301 rheometer (Anton Paar, Graz, Austria) with SIPLI attachment [47]. The rheometer was equipped with a Peltier temperature controller composed of bottom-plate and top-hood heaters, and plate-plate geometry (comprising of polished stainless-steel disk of 25 mm diameter and a fused quartz bottom plate). The SIPLI attachment, based on reflective polariscope principles, uses components of the parallel-plate geometry where the bottom (static) transparent plate and the top (rotating) reflective disk are parts of the optical setup allowing time-resolved reflected polarized light images (PLI) of measured samples to be recorded during shear. Descending shear

rate ($\dot{\gamma}$) sweeps were performed from 500 s^{-1} to 0.1 s^{-1} at a constant temperature of 20 °C, with a sample thickness (gap between the parallel plates) of 1 mm. All samples were measured at a concentration of 10 w/w % in water (without removal of insoluble material). During shear sweeps, imaging of the modified cellulose samples under crossed polarizers was performed to identify birefringent samples. The second set of experiments was performed at a constant angular speed of rotation, ω, of the shearing disk. In these experiments, the SIPLI technique was used to capture PLIs every second for 1000 s to observe the onset of orientation of the modified cellulose material under flow conditions. Since the shear rate experienced by each part of a sample in a parallel-plate geometry is proportional to its radial position ($\dot{\gamma} = \omega r / d$, where *r* is the radius of a corresponding sample position and *d* is the geometry gap), and assuming that the flow is laminar, SIPLI measurements at a constant ω enables birefringent properties of the sample to be tested within a range of share rates from 0 s^{-1} (at the sample center) to $\dot{\gamma}_{max} = \omega R / d$ (at the sample edge where *R* is the sample radius) simultaneously in a single experiment.

2.10. Molecular dynamics (MD) simulations

Theoretical tools such as MD simulations are useful for studying properties of cellulosic materials [48–53]. This technique provides information at spatial and temporal resolutions that would otherwise be inaccessible to experiment and, thus, can complement the experimental work. This technique is based on numerically solving Newton's equations of motions to describe the forces between atoms. In addition to extensive experimental studies, MD simulation is a suitable method for studying the properties of functionalized nanocellulose [48]. In the current work all MD simulations were performed using the molecular dynamics software LAMMPS

[54] with a velocity-Verlet integrator and an integration time step of 2 fs. MD simulations were conducted in the isothermal-isobaric (NPT) ensemble under constant temperature and pressure using Nose-Hoover thermostat and barostat with relaxation times of 0.2 ps and 2.0 ps, respectively. The Lennard-Jones interactions were switched to zero between 0.8 nm and 1.2 nm. The real space electrostatic interactions were cut off at 1.2 nm, while the long-range electrostatic interactions were evaluated using the particle-particle particle-mesh (P3M) method. Bonds and angles in water, as well as bonds involving hydrogen and any other atom, were kept rigid using the SHAKE algorithm with the relative tolerance of 10^{-4}. To describe the interactions between atoms the CHARMM all-atom additive force field (c36) [55,56] was used for carbohydrate part and the CHARMM General Force Field (CGenFF) [57] was used for substituents. Water was represented using the TIP3P model. Simulations were performed using oligomers containing 10 repeat units in the backbone. Four different samples were selected for simulations: unmodified cellulose, $C_{7/25}$, $C_{27/8}$ and $C_{50/0}$ (Table 1). The simulations began with preliminary constructed clusters consisting of 25 oligomer chains, solvated by water in a 0.125 nm^3 cubic box. The systems were equilibrated at room temperature before a mechanical force dipole of either 70 or 350 pN was applied to the ends of the oligomer chains, a method which has been established in our previous work [58]. For the calculation of hydrogen bonds, geometrical criteria based on the classical work of Luzar and Chandler: distance (D-A) ≤ 0.35 nm and angle (D-H-A) ≤ 30° were utilized [59]. The MD results were mainly analyzed using VMD software [60].

2.11. Thermodynamic integration (TI) technique

The change in Helmholtz free energy of hydration Δ*F*, the energy to transfer the unmodified glucose, glucose with the functional groups – HP and HPTMAC –

from their vapor phases to water, was calculated using TI technique as implemented in Materials Studio (BIOVIA) [61] (COMPASS force field, NVT ensemble, P = 1 atm, T = 298 K). In this method, the solute/water interaction is gradually increased from zero to full interaction in 21 steps, i.e., glucose or its modifications are gradually "grown" into water. For each coupling strength, Λ ranging from zero to unity, a simulation is performed and the derivative of the ΔF is calculated, and the free energy is obtained as the integral $\Delta F = \int_{\Lambda=0}^{\Lambda=1} \left\langle \frac{dH(\Lambda)}{d\Lambda} \right\rangle d\Lambda$, where H is the parameterized Hamiltonian. The hydration free energy was further calculated as a sum of three terms – "ideal", van der Waals and electrostatic contributions, as described elsewhere [62]. At each Λ value, 10 ns MD run was performed to equilibrate the systems composed of one solute molecule and 1000 water molecules. For the HPTMAC modified glucose, a Cl anion was added to keep the electroneutrality. For each molecule, three independent calculations of ΔF were performed.

3. Results & Discussion

Modification of native cellulose with the functional groups (HP and HPTMAC) were performed to different extents to give a series of modified cellulosic samples (Table 1 and Figure 2). For example, to produce the $C_{27/8}$ sample, 27 % of the pendent cellulose hydroxyls (targeting, on average, less than one of three units per AGU) were functionalized with HP and 8 % with HPTMAC, to give an overall degree of modification of 35 %. These two functional groups were chosen due to their proven capability in increasing the aqueous solubility of cellulosic material [38,63,64]. Hydroxypropyl groups provide steric hindrance to cellulose crystallisation, which can improve the water solubility of cellulose by interrupting the intra- and intermolecular hydrogen bonding throughout the sample [65–67]. The subsequent modification

group, (2-hydroxypropyl)trimethylammonium chloride, similarly introduces steric hindrance to the system but also establishes a large charge hindrance to cellulose crystallisation by introducing electrostatic repulsion between the cellulose chains. For example, this cationic substituent has been used to significantly improve the water solubility of high molecular mass glucan (M_w = 189 kDa) in water at MS_{cat} > 0.16 [35]. It is expected that both these processes cause cellulose chains to, preferentially, form hydrogen bonds with solvent molecules [38,63].

An analysis of the modified products by ^{1}H and ^{13}C NMR confirms the presence of either HP or HP and HPTMAC functional groups in the corresponding modified products and show a close correlation of the polymer composition measured from the NMR spectra to the targeted degree of modification (Figures S1 and S2). The molar (or degree of) substitutions of the hydroxypropylated samples determined with CP/MAS ^{13}C NMR were 0.2 (or 7 %) ($C_{7/0}$), 0.77 (or 26 %) ($C_{27/0}$), 1.41 (or 47 %) ($C_{50/0}$) and 2.35 (or 78 %) ($C_{80/0}$), which are in a good agreement with the expected MS_{HP} (or DS_{HP}) values (Figure S1).

NMR and elemental analysis of the HPTMAC-modified samples showed small variations of measured MS_{cat} from the targeted values (Figure S2 and Table S1). In particular, this was observed for samples targeted with the same HPTMAC DS where equivalent amounts of the cationization reagent had been used. For example, the measured ^{1}H NMR DS_{cat} of $C_{27/8}$ sample was 13 %, but for $C_{50/8}$, the DS_{cat} value was 8.5 % yielding an average of 10.8 %. Elemental analysis results were in agreement with ^{1}H NMR, with DS_{cat} values of 13 % and 8 % for $C_{27/8}$ and $C_{50/8}$ respectively, with an average of 10.5 %. The cellulosic samples targeted with 25 % HPTMAC were also shown to have variations in the resulting DS_{cat} values. ^{1}H NMR analysis shows DS_{cat} values of 16.9 %, 34.5 % and 22.9 % for the samples $C_{7/25}$,

$C_{27/25}$ and $C_{50/25}$, respectively, which gives an average DS_{cat} of 25 %. The DS_{cat} values from elemental analysis give a similar average of 24 %, with respective values of 24.7 %, 28.0 % and 18.7 %. For clarity of labelling, however, only the targeted DS values, expressed as percentages, are used for the sample codes (Table S2). The comparable results between the two methods show the successful incorporation of HPTMAC, which can be quantified by either ^{1}H NMR or elemental analysis producing consistent results.

Table 1. Overview of modified cellulose samples with their corresponding degrees of HP and HPTMAC substitution (DS_{HP} and DS_{cat}). For example, a sample with 50 % HP and 8% HPTMAC modification is labelled as $C_{50/8}$ and is located in the third column and second row of the table. *N.P.* stands for not possible, and *N.S.* stands for not synthesized.

		DS_{HP} / %			
		7	**27**	**50**	**80**
DS_{cat} / %	**0**	*Insoluble*	$C_{27/0}$	$C_{50/0}$	$C_{80/0}$
	8	*Insoluble*	$C_{27/8}$	$C_{50/8}$	*N.S.*
	25	$C_{7/25}$	$C_{27/25}$	$C_{50/25}$	*N.P.*

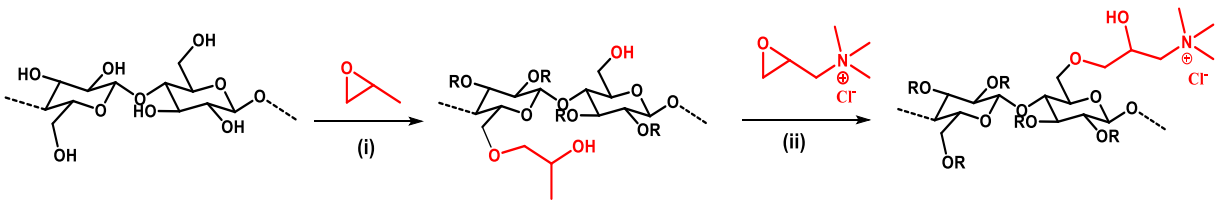

Figure 2. A route used for the cellulose modification: (i) hydroxypropylation with propylene oxide (PO) [R = $CH_2CH(OH)CH_3$, H] and (ii) following cationization with (2,3-epoxypropyl)trimethylammonium chloride (EPTMAC) [R = $CH_2CH(OH)CH_3$, H or $CH_2CH(OH)CH_2N(CH_3)_3Cl$].

Centrifugation measurements show a general decrease in solid content as the degree of pendent hydroxyl substitution increases (Figure 3). This is related to a

higher degree of water solubility of the modified cellulose. However, the observed solubility behavior was not solely due to the total increased modification of the cellulose chains. There is a pronounced trend associated with the degree of substitution indicating a strong effect of the hydroxypropyl units on the disruption of intra- and intermolecular hydrogen bonds within the cellulose system, resulting in the higher proportion of solvent-cellulose hydrogen bonds. The HPTMAC may also contribute to the cellulose aqueous solubility: modification of the $C_{27/0}$ with 8 % of HPTMAC ($C_{27/8}$) reduces the solid content from 53 % to 29 % (Figure 3). However, a further increase of the HPTMAC proportion ($C_{27/25}$) does not seem to have an effect on the overall water solubility of the cellulose chains (Table S2). $C_{27/8}$ and $C_{27/25}$ show similar amounts of solids (29 % and 36 %, respectively), despite a three-fold increase of HPTMAC substitutes. But in the case of a cellulose sample with a higher content of HP which was further modified by HPTMAC, $C_{50/8}$ and $C_{50/25}$ samples, the solubility in water is much higher as the amount of non-soluble materials is only a few percent (Figure 3 and Table S2). This indicates that the effect of hydroxypropyl group on the modified cellulose solubility in water seems to be more pronounced. This behavior could be due to the bulky HPTMAC groups targeting available hydroxyl sites either on the molecules initially solubilized by the HP groups or the surface of large aggregates, which is not as effective in solubilizing cellulose molecules. This conclusion is also supported by the fact that the HPTMAC modified cellulose with the largest disagreement between targeted and measured DS_{cat} values (the first three compositions in Table S1) contains the highest solids content (Table S2).

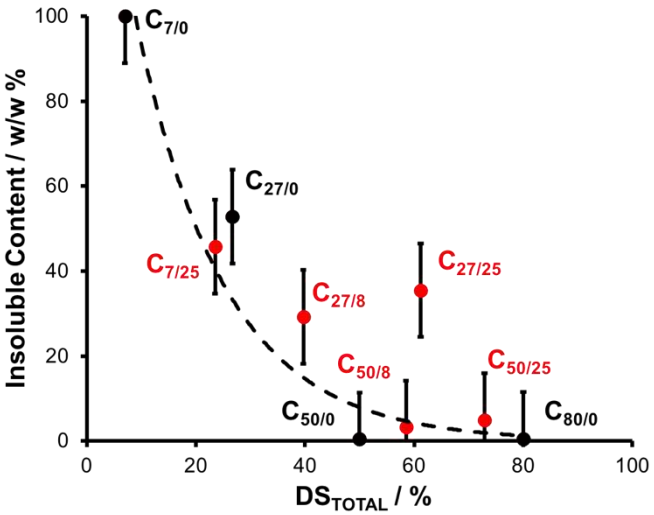

Figure 3. The proportion of water insoluble, solid material in 5 w/w % dispersions of modified cellulosic samples, plotted against the total degree of substitution (DS_{TOTAL}) [black and red symbols correspond to HP, and HP and HPTMAC modified cellulose, respectively, DS_{TOTAL} is calculated using the actual DS_{HP} and DS_{cat} (measured by ^{1}H NMR) values]; showing a rapid decrease in the solid content with an increasing proportion of HP group present. All measured points are labelled with the corresponding sample name. The dashed curve is plotted for guidance. The error bars represent standard error of the mean.

The modification of cellulose by ionic HPTMAC was further verified by zeta potential (ξ) measurements performed at 0.1 w/w % in the presence of 1mM KCl (Figure 4). The results confirm the presence of the positive electrokinetic potential for all cellulose samples modified by HPTMAC cationic group. Samples modified only with the hydroxypropyl group displayed no cationic charge, regardless of the degree of substitution. A clear trend can be seen in the ξ values; as the degree of HPTMAC present increases, the ξ value increases (Figure 4 and Table S2). Both series of samples with HP of 27 % and 50 % show a steady increase of the potential upon the increase of HPTMAC substituent content. Thus, in addition to the NMR results demonstrating a reasonably good correlation between the targeted cellulose modification and the sample composition, ξ-potential data further confirms the successful incorporation of the HPTMAC cationic group on to the cellulose.

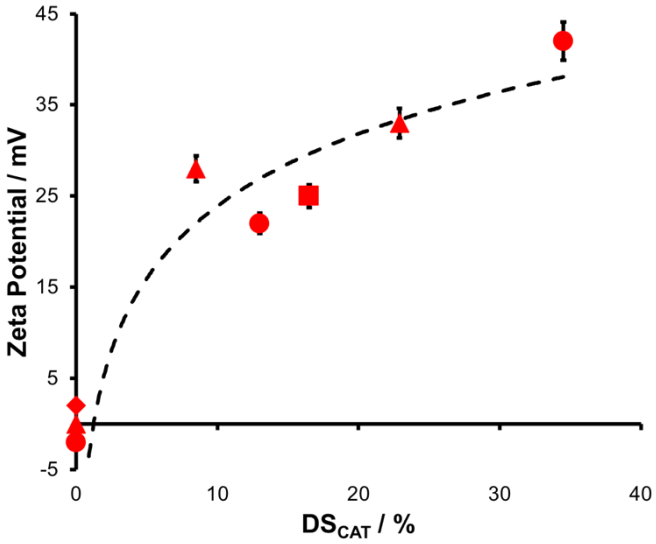

Figure 4. Zeta potential of modified cellulose samples plotted *versus* HPTMAC degree of substitution (DS_{cat}, measured by ^{1}H NMR). The data points were measured at 25 °C for 0.10 w/w % dispersions in the presence of 1 mM KCl. Error bars signify a 95% confidence interval. Data points for the samples with HP substitution of 7 % (square), 27 % (circle), 50 % (triangle) and 80 % (diamond) are shown. The dashed curve is plotted for guidance.

Two complementary techniques, TEM and SAXS, were used to assess structural morphology of the modified celluloses. While direct imaging by TEM provides detailed local information on shape and size of particles and aggregates, SAXS is a more statistically robust technique averaging information over a larger sample volume and evaluating structural organization of matter *in situ*.

All TEM images showed the presence of cellulose nanoparticles (CNPs) of a needle-like shape (Figure 5) indicating a similar morphological composition of the modified cellulose samples. The CNP mean length was around 100 nm with a relatively broad length distribution (Table S2) and is of a typical size range observed for nano-particulates derived from cellulose by various techniques such as acid [68,69] or enzymatic hydrolysis [70], treatment with eutectic solvents [71,72] and micromilling [73]. The TEM images demonstrate a good correlation with the solid

content measurements (Figure 3 and Table S2). In particular, TEM images of cellulose samples with the degree of substitution by HP equal to or more than 50 % (Figures 5d and 5f-5h), which were characterized by a very low solid content (Figure 3), show the presence of individual needles with no signs of aggregation. In contrast, the samples with HP content of 27 % or less (Figures 5a-5c and 5e), with a significant amount of insoluble solids (Figure 3), show the presence of aggregates composed of needle-like objects. Thus, increasing the degree of modification, especially by HP substitution, does indicate an increased aqueous solubility of the CNPs which can be seen in the absence of large aggregates in the TEMs of samples with HP content of 50 % and above. However, an increase of HPTMAC in the modified cellulose composition also improves the material's aqueous solubility which can be clearly followed using the samples with DS_{HP} of 27 % (compare Figures 5a, 5c and 5e). In this respect, it has to be concluded that the modification replacing the native hydroxyls impacts the formation of intermolecular hydrogen bonds and makes solvent-cellulose hydrogen bonding more favorable.

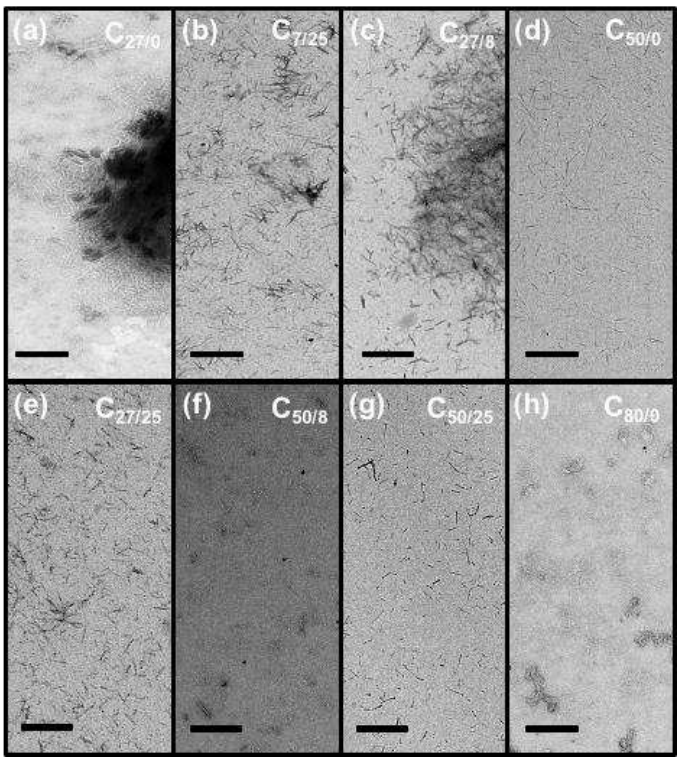

Figure 5. Representative TEM images of dried 0.10 w/w % aqueous dispersions of the modified celluloses: **(a)** $C_{27/0}$, **(b)** $C_{7/25}$, **(c)** $C_{27/8}$, **(d)** $C_{50/0}$, **(e)** $C_{27/25}$, **(f)** $C_{50/8}$, **(g)** $C_{50/25}$ and **(h)** $C_{80/0}$. The scale bar in each image corresponds to 500 nm.

X-ray scattering has proven useful in the characterization of modified cellulosic materials *in situ* by providing structural information averaged over thousands of particles [74], and in this respect, it is preferable to imaging techniques such as TEM. For example, Cameron *et al.* studied the modification of native cellulose with sodium hydroxide using SAXS [75], and Leppänen *et al.* utilized WAXS to find a relationship between the width of the cellulose crystals and the degree of extraction [76]. It is commonly accepted that polymer solutions or gels can be represented as two-component systems where the small-scale component represents single polymer chains, and the large-scale component represents possible aggregated multiple clusters formed by those chains. Thus, an equation for the intensity scattered by these systems is usually composed of two terms expressed via Lorentzian associated with Ornstein-Zernike formalism (molecules)

and squared Lorentzian associated with Debye-Bueche formalism (clusters) [77–79]. However, other expressions for the terms could be used such as Debye function, which is analytically correct for Gaussian polymer chains [80], and a power-law function based on variations of Porod's law [81], respectively. This common approach has also been adopted for aqueous solutions of cellulose derivatives using the following generalized scattering equation [82]:

$$I(q) = (\Delta\rho)^2 \left[\frac{K_1}{(1 + q^2 R_{gc}^2)^2} + \frac{K_2 P(q)}{1 + K_3 \exp(-q^2 K_4^2)} \right] \quad (1)$$

where $\Delta\rho$ is the excess scattering length density of the polymer (cellulose derivative) in the solvent (water), and K_1, R_{gc}, K_2, K_3 and K_4 are fitting parameters associated either with the volume fraction of clusters or averaged local polymer volume fraction fluctuations caused by inhomogeneity of polymer aggregates, averaged size of the clusters or correlation length of the fluctuations, the averaged single polymer chain volume and polymer concentration, the strength of repulsive interactions between the polymer chains and the correlation length of the repulsions, respectively. $P(q)$ is the polymer chain form factor which, for the sake of simplicity, could be expressed as [83]:

$$P(q) = \left[\frac{1}{\nu U^{1/(2\nu)}} \gamma\left(\frac{1}{2\nu}, U\right) - \frac{1}{\nu U^{1/\nu}} \gamma\left(\frac{1}{\nu}, U\right) \right] \quad (2)$$

with the modified variable $U = (2\nu + 1)(2\nu + 2)\frac{q^2 R_{gm}^2}{6}$, where R_{gm} is the averaged radius of gyration of molecules in solution, ν is the excluded volume parameter and $\gamma(s, x) = \int_0^x t^{s-1} \exp(-t) dt$ is the lower incomplete gamma function.

The terms of eq 1 are independent of each other and represent two populations of structural objects where the larger objects (characterized by R_{gc}) and the smaller objects (characterized by R_{gm}) produce asymptotic scattering signals at high q-values, described by power functions with exponents of -4 and close to -2, respectively. In case of polysaccharide systems studied for their response to different environments [82,84], the first term of eq 1 was assigned to assemblies of polymer chains which may attract each other and/or form entanglements. The second term of eq 1 was assigned to the macromolecules distributed over the whole system homogeneously where the structure factor of Gaussian form describes the possible repulsive interactions among the polymer chains and an existence of correlation distance between the chains. This approach enabled transformation in the systems to be followed by SAXS, from a state of associated molecules to a completely dissolved state through various intermediate stages. In this respect, eq 1 could also be used for analyzing cellulose modified by HP and HPTMAC groups which could lead to either partial or complete dissolution.

If molecules dissolved in a solution are not strongly interacting and/or their concentration is low ($K_3 = 0$), eq 1 is simplified to [82,85]:

$$I(q) = (\Delta\rho)^2 \left[\frac{K_1}{(1 + q^2 R_{gc}^2)^2} + K_2 P(q) \right] \qquad (3)$$

Alternatively, for systems containing dissolved molecules with strong interactions of a repulsive nature the first term of eq 1 should be neglected, reducing the scattering equation to the second term only.

The scattering equation based on two populations of scattering objects (eq 3) produced reasonably good fits to experimental SAXS patterns of the modified

cellulose 1 w/w % aqueous solutions (Figure 6). The SAXS analysis (Table 2), in combination with TEM observations, shows that upon an increase of the hydroxypropyl group content in the modified cellulose the large object (aggregate) size reduces from tens of microns, detected by TEM for insoluble aggregates of $C_{7/0}$, to about 30 nm for $C_{50/0}$ and to virtually zero, a complete solubilization of the objects undetectable by SAXS, for $C_{80/0}$. In addition, a trend of decreasing size can be identified for the large objects upon increase of the HPTMAC group content. For example, SAXS results suggest that large insoluble aggregates of $C_{7/0}$ reduce to micron size for $C_{7/25}$ and the same increase of the HPTMAC group content from 0% for $C_{50/0}$ to 25% for $C_{50/25}$ makes the large objects fully solubilized, and undetectable by SAXS (Table 2). TEM images indicate a presence of needle shaped CNPs (Figure 5). The radius of gyration of a rigid rod is expressed as $R_g^2 = \frac{L^2}{12} + \frac{R_r^2}{2}$, where L and R_r correspond to its length and cross-section radius, respectively [86], which reduces for needle-shaped objects with a large aspect ratio ($L \gg R_r$) to $R_g^2 \approx \frac{L^2}{12}$. A comparison of the radius of gyration for the large objects measured by SAXS (R_{gc}) and the CNP length obtained by TEM (L), performed using this relationship, shows a reasonably good correlation (Table 2). This result suggests that the large objects detected by SAXS for most of modified cellulose materials are CNPs. It might be expected that the CNPs were composed of crystalline cellulose [2]. However, WAXS patterns of the modified cellulose samples, simultaneously recorded with SAXS data, are represented by a broad peak at q ~ 16 nm^{-1} (Figure S3) which is commonly observed for amorphous cellulose [87]. There were no well-defined diffraction peaks which could be associated with crystalline cellulose. Thus, WAXS results indicate that the modified cellulose is mainly in an amorphous state and, possibly, the

scattering measurements are not sensitive to the small fraction of crystalline material in the needle-shaped cellulose nanoparticles. The combined analysis of solid content (Figure 3), TEM (Figure 5) and SAXS (Figure 6 and Table 2) results shows that cellulose aggregates, virtually insoluble in water at small level of substitution by HP (DS_{HP} = 7 %), disintegrate into CNPs at intermediate levels of cellulose modification by HP and HPTMAC, followed by a complete solubilization at extreme, high DS value, conditions (Figure 3 and Table 2, $C_{80/0}$).

A reduction of the large object population fraction, correlated with the solid content (Figure 3), was accompanied by a relative increase of the small object population fraction related in the scattering equation to dissolved molecules (eq 3). Since molecules cannot be detected by TEM, characterization of the modified cellulose by SAXS is more preferable in this case. SAXS analysis shows that the second population is represented by molecules with the radius of gyration (R_{gm}) in a range of 20 nm (Table 2). There is a gradual increase of R_{gm} with increasing DS_{HP}. Possibly, small cellulose molecules are more prone to the modification, resulting in a smaller R_{gm} for celluloses with a lower degree of modification. At $DS_{HP} \geq 50\%$, when most of the molecules are modified, including high molecular weight cellulose, the averaged R_{gm} appears larger. SAXS results further indicate that for $DS_{HP} \leq 27\%$ the excluded volume parameter, ν, is less than 0.5 (Table 2). This suggests that for celluloses with a low degree of substitution, water remains a relatively poor solvent. As such, and according to solid content results (Figure 3) and TEM (Figure 5), the modified celluloses still form large aggregates. As the degree of substitution increases, ν also increases to the point where water becomes a good solvent ($\nu >$ 0.5) for the modified cellulose samples leading to a larger proportion of free CNPs (Figure 5) and molecules in solution. In particular, no aggregates or large objects are

detected by SAXS for $C_{50/25}$ and $C_{80/0}$ where ν reaches 0.59 and 0.55, respectively (Table 2). It would be interesting to compare the measured R_{gm} values with values calculated for the studied molecules using equation based on general principles of polymer physics [83]:

$$R_{gm}^2 = \frac{b^{2(1-\nu)} L_{mol}^{2\nu}}{(2\nu+1)(2\nu+2)} \quad (4)$$

where L_{mol} is the total contour length of the polymer chain and b is the Kuhn length. Considering that molecular weight and length of the AGU is 162 Da and 0.52 nm [88], respectively, and the polymer molecular weight after the modification remains approximately the same (78 kDa was detected by GPC for $C_{50/0}$), L_{mol} = 78 kDa/162 Da × 0.52 nm ≈ 250 nm. Thus, assuming *theta*-solvent conditions (ν = 0.5) and that b of the modified cellulose molecules is 15 nm, based on commonly accepted values for cellulose and its derivatives being in a range of 10 – 20 nm [89–92], the R_{gm} of a single molecule, calculated from eq 4, is about 25 nm. Considering the number of assumptions made, the estimated R_{gm} value is in a good agreement with the R_{gm} values measured by SAXS (Table 2). This comparison suggests that increasing the degree of cellulose modification enables aggregates and/or CNPs to be dissolved into their constitutive molecules.

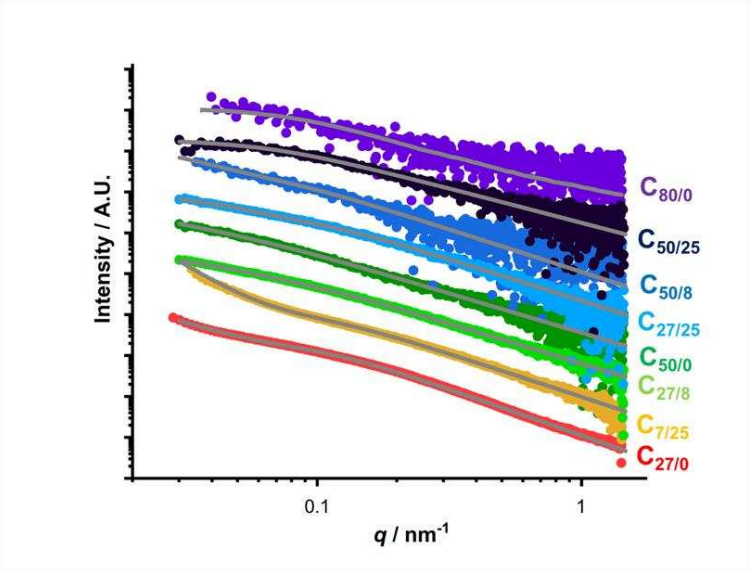

Figure 6. Double logarithmic plot of representative SAXS patterns of 1.0 w/w % modified cellulose aqueous dispersions (symbols). The grey lines show the fitted model, using an established two-population model for cellulose (eq 3). The SAXS patterns are offset for clarity.

Table 2. Summary of structural parameters obtained by fitting scattering equation (eq 3) to SAXS patterns of the modified cellulose samples (Figure 6), with R_{gc} and R_{gm} corresponding to the radius of gyration of large cellulose objects (aggregates) and small objects (molecules), respectively, and ν is the excluded volume parameter. L is the length of CNPs measured from TEM images (Figure 5).

		DS_{HP} / %				**Structural Parameters**
		7	**27**	**50**	**80**	
DS_{cat} / %	**0**	*Insoluble*	0.44	0.52	0.55	ν
			40.9	30.6	-	R_{gc} / nm
			14.9	23.5	25.6	R_{gm} / nm
			138 ± 33	122 ± 28	-	L / nm
	8	*Insoluble*	0.48	0.51	*Not Synthesized*	ν
			21.2	31.8		R_{gc} / nm
			15.4	19.0		R_{gm} / nm
			100 ± 29	118 ± 40		L / nm
	25	0.47	0.49	0.59	*Not Possible*	ν
		1029.4	21.0	-		R_{gc} / nm
		13.4	13.9	21.6		R_{gm} / nm
		109 ± 31	101 ± 35	91 ± 34		L / nm

Based on the results of structural characterization techniques, it can be concluded that increasing the degree of substitution gradually changes the

cellulose's water solubility leading to the formation of different morphologies upon dispersion and solubilization in water. At low DS_{HP} (7 %) the modified cellulose appears mainly as large aggregates (Figure 7a). An increase of the HP component, also accompanied by HPTMAC substitution, to a moderate level (DS_{HP} = 27 %) leads to a partial destruction of the aggregates into CNPs and single modified cellulose molecules (Figure 7b) followed by a full disintegration of the aggregates at higher DS_{HP} (50 %) (Figure 7c) which is completed by a molecularly dissolved material at the higher end of the total substitution (Figure 7d).

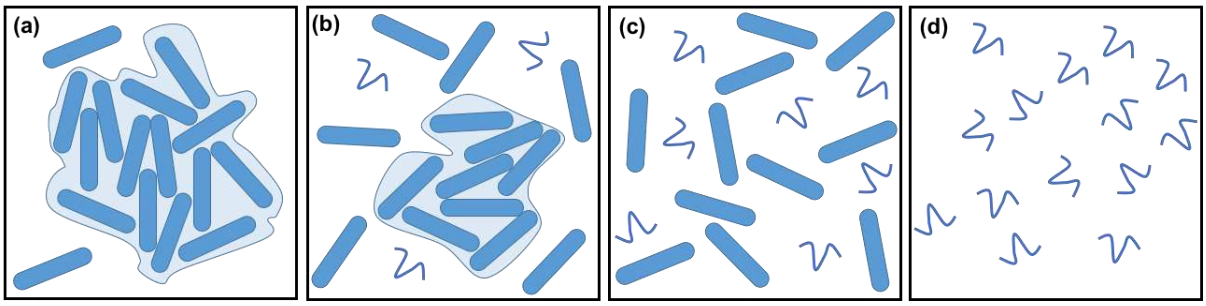

Figure 7. Schematic representing the fragmentation of aggregates with increasing modification: (a) presence of large aggregates with a few loose particles at low degrees of modification; (b) intermediate degrees of substitution with smaller aggregates present, a greater population of free CNPs and a small proportion of single molecules; (c) CNPs and molecules with no aggregates present at higher degrees of modification and (d) only molecules are present at the highest degrees of modification.

A number of optical and rheological techniques are effective for a characterization of cellulosic products. Despite the high volume of work published on measuring and understanding the cellulose birefringence (over 1000 papers in 2019 alone), most of these are performed on final products such as thin films or fibers after some type of material processing [93–95]. However, birefringence-based techniques could be appropriate for studying cellulosic materials, especially soluble in water, during processing. In this respect, SIPLI [96] could be suitable to monitor (without destruction) reversible and irreversible changes in cellulosic samples under

shear flow. Rheo-optical measurements were carried out using rotational (shear) rheology combined with *in situ* polarized light imaging (SIPLI setup) in order to investigate the rheological and birefringent properties of the eight modified samples. Initially, experiments were performed to determine the shear-rate dependent viscosity of the samples, and to investigate whether the samples were birefringent. It was found that three of the modified celluloses with the highest DS_{TOTAL} ($C_{50/8}$, $C_{50/25}$ and $C_{80/0}$) displayed low apparent viscosity (term "apparent" is used to emphasize that parallel-plate rotational geometry was applied for the measurements; however, this will be omitted in the following text) (Figure 8). This is due to a high proportion of substituted hydroxyl groups leading to good solubility of these cellulose derivatives in water (Figure 7d) as indicated by TEM, SAXS and solid content measurements (Table S2). This is also supported by the fact that the sample with the lowest DS_{TOTAL} in this group ($C_{50/8}$) is the most viscous. Shear thinning behavior observed for these samples at high shear rates is likely to be associated with the elastic properties of the dissolved molecules. The remaining five modified cellulose samples ($C_{27/0}$, $C_{27/8}$, $C_{7/25}$, $C_{50/0}$ and $C_{27/0}$) displayed shear-thinning behavior with low-shear-rate viscosity up to two orders of magnitude higher than for the samples with a higher degree of solubilization. This rheological result indicates strong elastic properties of cellulosic material with partially substituted hydroxyl groups. The shear thinning observed over a wide range of shear rates suggests that the material is composed of objects with both short and long relaxation times which could be indicative of a polymer and particle network formation. However, considering a mixed morphology of the samples (Figures 7a-7c) and a combination of factors which could affect sample viscosity (such as anisotropic CNPs, electrostatic repulsions among the cationic side chains, and inter-cellulose and cellulose-water hydrogen bonding

connectivity), it would be difficult if not impossible to perform a detailed interpretation of the observed results. Nevertheless, the rheological measurements show that there is a striking change of viscoelastic properties of the modified cellulose: upon reaching high level of hydroxyl group substitution by HP or HP and HPTMAC the material turns into a low-viscous fluid (Figure 8) due to the complete solubilization of the constituent cellulose chains (Figure 7d).

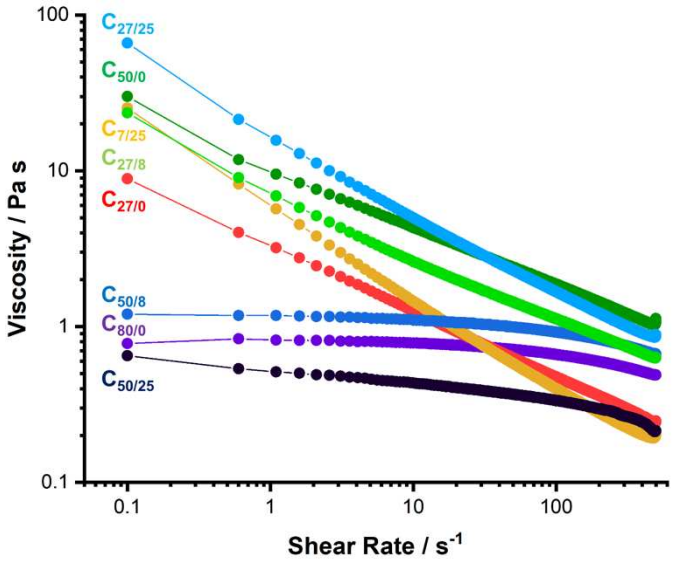

Figure 8. Apparent viscosity *versus* shear rate profiles for all samples between 500 – 0.1 s^1 at a constant temperature of 20 °C. All samples were measured at a concentration of 10 w/w %. Since parallel-plate rotational geometry was applied for the measurements, an "apparent viscosity" term is used. The shear rate values correspond to the disk edge.

The second part of rheo-optical results represented by PLI observations of the sheared samples has demonstrated that samples of modified cellulose corresponding to intermediate degree of substitution could be birefringent. Indeed, PLIs of $C_{50/0}$, $C_{27/25}$ and $C_{50/8}$, recorded at a constant angular speed using SIPLI, exhibit a Maltese cross pattern (Figure 9) characteristic of a birefringent material aligned along the flow direction [47,96]. Birefringent properties are commonly described by an optical indicatrix (ellipsoid of electro-magnetic wave normal)

representing the refractive index values for all directions of light (electric field vector) vibrations propagating through a material [97]. The optical indicatrix of a viscoelastic liquid is usually represented by a sphere, all directions are equivalent in the space, and as a result the material is isotropic and no birefringence is observed. However, the impact of flow could cause deformation and/or orientation of objects in the liquid, transforming the spherical optical indicatrix into an ellipsoidal one by introducing an uniaxial anisotropy associated with birefringence [47,98]. When the ellipsoid principal axis forms a zero angle with the polarizer or analyzer axis, an extinction pattern similar to Maltese cross appears in PLIs.

$C_{50/0}$ demonstrated a very pronounced Maltese cross through the entire sample (sheared in a parallel-plate geometry) indicating that the material becomes birefringent virtually over the whole range of shear rates used. Since the material can be aligned at relatively low shear rates, this suggests that large objects with long relaxation times are involved in the formation of an oriented morphology producing birefringence. This sample is mainly composed of non-aggregated CNPs and dissolved cellulosic molecules (Figure 5, Table 2 and Figure 7c). The material has not been fully solubilized at a molecular level but the degree of substitution does not allow large aggregates to be formed in water solution either. At the same time the material shows shear thinning behavior over the entire range of share rates used for the SIPLI experiment (Figure 8), also indicating a presence of viscoelastic objects with a long relaxation time. It is expected that the CNPs and cellulosic molecules coexist in the water solution and interact with each other via hydrogen bonds to form a polymeric/particle network which orients under a shear along the flow directions resulting in the material birefringence. The half-life of the Maltese cross intensity decay after cessation of shear calculated using the previously established protocol

[99] indicated that the network formed has a relaxation time of approximately 9 s. These aligned structures could act as a precursor for the formation of a fibrous cellulose under a flow processing from a water solution.

In contrast, the cellulosic materials corresponding to both low and high degrees of substitution (DS_{TOTAL} < 52% and DS_{TOTAL} > 58%, respectively) demonstrated no signs of birefringence (Figure 9) suggesting that no structure with a preferable orientation is formed under shear. Considering morphologies formed by these cellulosic materials (Figures 7a and 7b, and Figure 7d, respectively), the causes of this non-birefringent behavior should be different. The highly modified cellulose forms an aqueous solution of molecules (Figure 7d) of a relatively low molecular weight (M_w = 78 kDa) with fast relaxation times (less than 0.01 s) which cannot be aligned at the accessible shear rates in the instrument. Furthermore, they do not form inter-molecular bonds to create larger objects (molecular networks) which could be oriented under the flow processing, as indicated by a low viscosity (Figure 8). For these reasons, the samples not only remain unaligned by the shear rates used ($\dot{\gamma} \leq 100$ s^{-1}) but also do not form large orientable objects (molecular networks), hence no birefringence-related effects (absence of Maltese cross) are observed (Figure 9). The celluloses with lower levels of substitution comprise of a mixture of morphologies spread over a wide range of scales (Figures 7a and 7b). Although these materials demonstrate a high viscosity similar to the highly birefringent $C_{50/0}$ (Figure 8), this is mainly caused by a presence of partially solvated (swollen) large aggregates (Figure 5 and Table 2), which also could be the cause of the slight turbidity in these samples in comparison with the transparent samples of highly modified cellulose (Figure 9). Perhaps, the different morphologies present at this level of DS_{TOTAL} cannot create stable interactions that would drag the aggregates

of a uniform shape into the formation of a stable network aligning under the flow processing. As a result, the material appears non-birefringent in the SIPLI measurements (Figure 9).

With the exception of $C_{50/0}$, the modified cellulosic samples were found to display very weak or no birefringence under shear conditions (Figure 9). At low DS_{TOTAL} ($C_{7/25}$, $C_{27/0}$ and $C_{27/8}$), the samples remain heterogeneous due to the presence of large aggregates and show no structural orientation under shear conditions. However, upon the increase of HPTMAC substitution ($C_{27/25}$) the aggregates are significantly destroyed (Figure 5e) and the sample becomes more homogeneous with an ability to form a polymeric network evident by an appearance of structural orientation (Maltese cross) under flow conditions (Figure 9, $C_{27/25}$). When the modification exceeds a significant amount, the water solubility of the cellulosic material is high, due to preferential hydrogen bonding with solvent molecules over cellulose chains. These impacts lead to liquid-like behavior under small shear rates (Figure 8, samples $C_{50/8}$, $C_{50/25}$ and $C_{80/0}$), with little ($C_{50/8}$) to no alignment ($C_{50/25}$ and $C_{80/0}$) observed during SIPLI measurements (Figure 9).

There is a clear relationship between the sample orientation under shear flow, highlighted by birefringent properties, and the cellulose modification targeted during synthesis. A medium amount of substituted AGU hydroxyl groups (between 50 – 58%) leads to the formation of a flow-induced birefringence detectable by the presence of a Maltese cross (Figure 9). It is thought to be due to a ‘sweet spot’ in modification of hydroxypropyl functional groups, where the derived morphology (Figure 7c) leads to good solubility in water, yet intermolecular hydrogen bonding between cellulosic objects/molecular chains is still favorable, forming a macroscopic oriented structure under shear. This is promising behavior for fiber formation, the

recent review of lower critical solution temperature behaviour of modified celluloses by Coughlin *et al*. indicates that phase separation is driven by nano-fibril formation in soluble cellulosic materials [100]; the mechanism proposed involves polymer chains becoming aligned on the length scale of a few AGUs to form nuclei and then those nuclei growing into aligned fibrils, and such a mechanism would clearly be accelerated by elongational flow. In order to verify this hypothesis, samples representing different morphologies detected by SAXS and other techniques (Figure 7) have been tested for fiber formation using a dry spinning device comprised of a dosing syringe pump and a spinning cylinder [101,102]. This fiber spinning technology was developed at Spinnova (Jyväskylä, Finland). An aqueous dispersion is dosed using a syringe pump with a desired feed flow through a nozzle onto the surface of a rotating cylindrical drum (Figure S4). The linear velocity of the drum surface (v_1), the nozzle jet speed (v_2) and the nozzle inner diameter can be adjusted depending on the dispersion dry solid content to achieve a desired fiber linear density. A material ability to tolerate differences between the nozzle jet speed and the drum surface speed (stretching ratio, v_2/v_1) determines its suitability for a successful spinning. The modified cellulosic materials herein required a relatively high drysolid content of 10 w/w % to enable successful fiber spinning. The fiber spinning was performed at ambient conditions (room temperature and relative humidity of 30-40%).

It was found that both moderately modified cellulose sample ($C_{7/25}$) corresponding to large or partially disintegrated aggregates (Figures 7a and 7b) and a molecularly dissolved material (Figure 7d) with a high degree of substitution ($C_{80/0}$) produced no fibers under spinning from an aqueous solution. In contrast, the cellulosic sample with an intermediate level of hydroxyl substitution ($C_{50/0}$)

representing a morphology with fully disintegrated aggregates (Figure 7c) and demonstrating strong flow-induced birefringence (orientation) (Figure 9), was capable to form fibers. Using optimized processing conditions set at v_1 = 5.77 m/s (the syringe feed flow of 12 ml/min through the nozzle inner diameter of 210 µm) and v_2 = 7 m/s, a $C_{50/0}$ 10 w/w % aqueous dispersion produced superfine fibers with a linear density of 2.86 tex, a tenacity of 6.19 cN/tex and an elongation of 4.88%. These preliminary data demonstrate a good correlation between the material processing requirements, such as spinnability and fiber formation, suitable for industrial applications and the results obtained by lab-based techniques. The approach presented, based on flow-induced birefringence/orientation of modified cellulose in solutions, could be an efficient tool for the development of processable cellulosic materials, but a full-scale study of this subject is beyond the scope of this work.

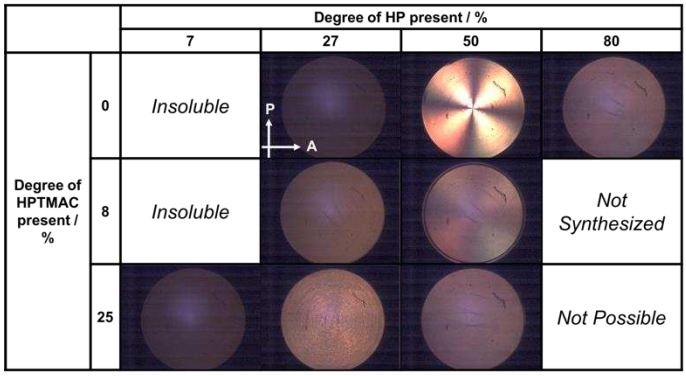

Figure 9. Shear-induced polarized light imaging (SIPLI) of 10 w/w % dispersions of all eight modified cellulose samples at 20 °C (parallel-plate geometry, disk diameter 25 mm, geometry gap 1 mm, angular speed 40 rad s^{-1} corresponding to a maximum shear rate of 100 s^{-1} at the sample edge. Selected PLIs represent the birefringent behavior of the samples at different degree of substitution. The white arrows on the PLI for $C_{27/0}$ indicate the direction of the polarizer (P) and analyzer (A) respectively for all images. A Maltese cross pattern indicates sample birefringence (shear-induced alignment), whereas the absence of such a pattern indicates no birefringence (no alignment).

In order to gain further insights into the structural organization of modified celluloses at a molecular level, MD simulations have been performed for native cellulose and three other samples ($C_{7/25}$, $C_{27/8}$ and $C_{50/0}$). These samples were selected along the composition matrix diagonal covering the wide range of HP and HPTMAC modifications (Table 1) to optimize time-consuming MD simulations (Figure 10). The use of MD simulations was to further understand the macroscopic observations seen in structural and rheo-optical measurements. The first simulation examined the degree of modification effects on the aqueous solubility. During the elapsed simulation time of 120 ns, the native cellulose oligomers remained in close contact with each other and did not show any sign of dissolution. This prediction was supported by the presence of a single broad peak in the intermolecular pair correlation function (PCF) between the residues of oligomer chains (Figure 10d, black trace). $C_{50/0}$ was found to be partially soluble, with some degree of close-contact interactions still present after the simulation (Figure 10d, red trace), which was consistent with the morphology detected by structural techniques (Figure 7c). In contrast, it was found that $C_{27/8}$ was primarily soluble, with sharply reduced correlations and $C_{7/25}$ fully dissolved in water without any close-contact interactions. This behavior is due to the increasing presence of the cationic modification group, HPTMAC, which leads to preferential hydrogen bonding between cellulose chains and water due to charge repulsion. On the microscopic level, this means that the chains are increasingly more soluble with the presence of this modification group. However, this is not observed on the macroscopic level due to the bulky HPTMAC groups which preferentially target the hydroxyls present on the surface of large cellulose aggregates (Figures 7a and 7b).

To quantify the increase in water solubility, the free energies of hydration Δ*F* for native glucose, HP, and HPTMAC modifications were calculated (Table 3). The HP modification leads to an increase in the aqueous solubility of cellulose chains. At the same time, longer HP side chains contribute to a sparser packing of the backbones as compared to the native cellulose. This increase in aqueous solubility has been seen experimentally (Figures 3 and 5). The modification of the repeat unit with a charged trimethylammonium group increases the aqueous solubility more than twice, as follows from the data. Moreover, the longer chain, and the presence of a charged group in HPTMAC should prevent the fiber formation. This has been seen experimentally for samples with high DS_{TOTAL} with no orientation observed by the rheo-SIPLI technique (Figure 9) and no fiber formation during spinning.

Table 3. Overview of results for all the simulated samples including native glucose and targeted modifications with HP and HPTMAC.

	Native glucose	**HP glucose**	**HPTMAC glucose**
Δ*F* / kcal mol $^{-1}$	-14.34	-14.93	-30.05
Std error / kcal mol $^{-1}$	1.13	1.21	1.20

To elucidate the impact of external forces on water solubility, the intermolecular pair correlation functions (PCF) between the residues of the four systems were calculated (Figures 10d and 10e). The presence of a single, broad peak for unmodified cellulose oligomers supports the conclusion drawn from WAXS measurements about the amorphous nature of the sample (Figure S3). The

application of force on $C_{50/0}$ resulted in increased correlation intensities. In this regard, it is worth noting that the appearance of oscillating peaks in the PCF indicates the formation of fibrillary nanoclusters. Given a sufficiently long time for the relaxation of stretched $C_{50/0}$ oligomers, the formation of a unified fiber is expected and supported by experimental results on spinning this cellulosic material. However, for the current time of 120 ns, there are certain differences in the correlation intensities and the shape of the PCFs for the two forces investigated. This implies that there may be some threshold force value, above which the oligomers become aligned along the force direction and can participate in the fiber formation. However, if the force applied is large enough, such as 350 pN, the complete straightening of the chains leads to the alignment of all backbone glucose residues in the same plane. As a consequence, the fiber formation undergoes a different reorganization and nucleation path. Compared to $C_{50/0}$, $C_{27/8}$ has sharply reduced correlations, and $C_{7/25}$ displays almost no correlations between the residues due to the nearly homogenous distribution of the chains. This can be explained in an increase in electrostatic repulsion between positively charged quaternary ammonium groups, eventually preventing the close-contact interactions between the chains; this is the case for $C_{7/25}$. The MD simulation results for the later sample are somewhat contradictory to the experimental data which suggests that $C_{7/25}$ contains a significant amount of aggregates (Figures 3, 5b, 6 and 7b). This apparent inconsistency is likely related to the fact that the modification of cellulose is inhomogeneous at small amount of HP causing restricted access for the HPTMAC modifier and resulting in a relatively high solid content after the modification (Figure 3).

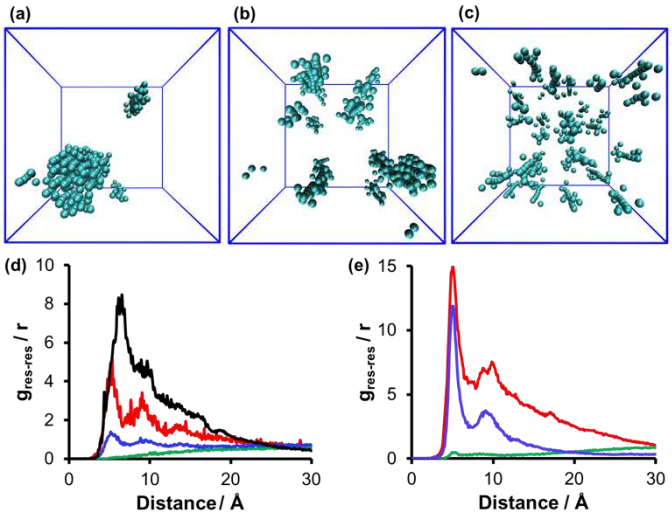

Figure 10. Snapshots illustrating the residue representation (water molecules are omitted for clarity) at 298 K of **(a)** $C_{50/0}$, **(b)** $C_{27/8}$ and **(c)** $C_{7/25}$. Two-dimensional intermolecular pair correlation functions (PCF) between the residues of native cellulose and modified cellulose oligomers at a time of 120 ns with **(d)** no force and **(e)** 350 pN of applied force. The results obtained for native cellulose, $C_{50/0}$, $C_{27/8}$ and $C_{7/25}$ are represented by black, red, blue and green traces, respectively.

4. Conclusions

A range of cellulose derivatives with different water solubility were formed by substituting the hydroxyl groups in the AGU of cellulose with varying amounts of hydroxypropyl groups, followed by further modification with a cationic component [(2-hydroxypropyl)trimethylammonium chloride]. A combination of techniques such as ^{1}H and ^{13}C NMR spectroscopy, zeta potential measurements and elemental analysis were used to characterize the material composition and the substitution by both hydroxypropyl and (2-hydroxypropyl)trimethylammonium chloride was confirmed.

The structural characterization techniques demonstrated that the increase of the degree of substitution gradually changes the solubility of cellulose in water leading to the formation of different coexisting morphologies. TEM and SAXS show that at low DS_{HP} (7 %) the modified cellulose is represented mainly by large aggregates. Upon increase of the HP component, and incorporation of HPTMAC substitution, to a moderate level of DS_{HP} (27 %), a partial destruction of the aggregates into CNPs and single modified cellulose molecules is observed. A full disintegration of the aggregates was detected at higher DS_{HP} (50 %) which was followed by a molecularly dissolved material at the higher end of the total substitution (DS_{TOTAL} > 75 %).

Rheo-optical measurements performed on the modified cellulose dispersions in water together with fiber-spinning results enabled a composition corresponding to DS_{HP} of 50 % to be identified as the most suitable for the fiber formation. In this respect, the SIPLI technique appeared to be an efficient tool for testing flow processability of the modified cellulose. It is expected that at DS_{HP} ~ 50 %, the CNPs and cellulosic molecules, coexisting in the water solution, interact with each other via

hydrogen bonds forming a molecule-particle network which orients under a shear along the flow directions. Thus, this aligned structure can potentially act as a precursor for the formation of fibrous cellulose from a water solution under flow conditions. It was also observed that the incorporation of a cationic modification group reduces the ability of material to form the fibrous morphology. This is thought to be due to the repulsion present between these ionic groups on the cellulosic backbone.

The obtained experimental results are underpinned by MD simulations. For the three representative samples considered in molecular dynamics simulations ($C_{7/25}$, $C_{27/8}$ and $C_{50/0}$), only $C_{50/0}$ showed evidence of the liquid-to-solid phase transition under stress. It was found that there is a threshold value of the simulated force applied, above which the cellulosic oligomers become aligned along the force direction and begin a co-operative process of fiber formation. These theoretical findings support the experimental rheo-optical results and are in a good correlation with the fiber formation observed during spinning the $C_{50/0}$ aqueous dispersion.

Acknowledgements

J.S., H.S., J.-U.S., A.J.R. and O.O.M. thank ERC for funding FLIPT project (Horizon 2020, EU project 713475). Diamond Light Source (Didcot, UK) and EPSRC (EP/L016281/1) are thanked for funding a CDT PhD CASE studentship for C.T.O'B. O.O.M. thanks EPSRC for the capital equipment grant to purchase the laboratory based Xenocs Xeuss 2.0/Excillum SAXS/WAXS beamline used for characterizing the modified cellulose aqueous solutions (EP/M028437/1).

References

[1] N. Lavoine, I. Desloges, A. Dufresne, J. Bras, Microfibrillated cellulose - Its barrier properties and applications in cellulosic materials: A review, Carbohydr. Polym. 90 (2012) 735–764. https://doi.org/10.1016/j.carbpol.2012.05.026.

[2] R.J. Moon, A. Martini, J. Nairn, J. Simonsen, J. Youngblood, Cellulose nanomaterials review: structure, properties and nanocomposites, Chem. Soc. Rev. 40 (2011) 3941–3994. https://doi.org/10.1039/c0cs00108b.

[3] Y. Nishiyama, J. Sugiyama, H. Chanzy, P. Langan, Crystal Structure and Hydrogen Bonding System in Cellulose Iα from Synchrotron X-ray and Neutron Fiber Diffraction, J. Am. Chem. Soc. 125 (2003) 14300–14306. https://doi.org/10.1021/ja037055w.

[4] A. Lu, U. Hemraz, Z. Khalili, Y. Boluk, Unique viscoelastic behaviors of colloidal nanocrystalline cellulose aqueous suspensions, Cellulose. 21 (2014) 1239–1250. https://doi.org/10.1007/s10570-014-0173-y.

[5] D. Bondeson, K. Oksman, Dispersion and characteristics of surfactant modified cellulose whiskers nanocomposites, Compos. Interfaces. 14 (2007) 617–630. https://doi.org/10.1163/156855407782106519.

[6] K. Tashiro, M. Kobayashi, Theoretical evaluation of three-dimensional elastic constants of native and regenerated celluloses: role of hydrogen bonds, Polymer (Guildf). 32 (1991) 1516–1526. https://doi.org/10.1016/0032-3861(91)90435-L.

[7] Y. Boluk, R. Lahiji, L. Zhao, M.T. McDermott, Suspension viscosities and shape parameter of cellulose nanocrystals (CNC), Colloids Surfaces A Physicochem. Eng. Asp. 377 (2011) 297–303. https://doi.org/10.1016/j.colsurfa.2011.01.003.

[8] M. Bergenstråhle, J. Wohlert, M.E. Himmel, J.W. Brady, Simulation studies of the insolubility of cellulose, Carbohydr. Res. 345 (2010) 2060–2066. https://doi.org/10.1016/j.carres.2010.06.017.

[9] N. Tulos, D. Harbottle, A. Hebden, P. Goswami, R.S. Blackburn, Kinetic Analysis of Cellulose Acetate/Cellulose II Hybrid Fiber Formation by Alkaline Hydrolysis, ACS Omega. 4 (2019) 4936–4942. https://doi.org/10.1021/acsomega.9b00159.

[10] S. Kushwaha, R. Singh, Suhas, M. Chaudhary, P.J.M. Carrott, V.K. Gupta, Cellulose: A review as natural, modified and activated carbon adsorbent, Bioresour. Technol. 216 (2016) 1066–1076. https://doi.org/10.1016/j.biortech.2016.05.106.

[11] S. Hokkanen, A. Bhatnagar, M. Sillanpää, A review on modification methods to cellulose-based adsorbents to improve adsorption capacity, Water Res. 91 (2016) 156–173. https://doi.org/10.1016/j.watres.2016.01.008.

[12] P. Tingaut, R. Hauert, T. Zimmermann, Highly efficient and straightforward

functionalization of cellulose films with thiol-ene click chemistry, J. Mater. Chem. 21 (2011) 16066–16076. https://doi.org/10.1039/c1jm11620g.

[13] D. Klemm, B. Heublein, H.P. Fink, A. Bohn, Cellulose: Fascinating biopolymer and sustainable raw material, Angew. Chemie - Int. Ed. 44 (2005) 3358–3393. https://doi.org/10.1002/anie.200460587.

[14] B. Lindman, G. Karlström, L. Stigsson, On the mechanism of dissolution of cellulose, J. Mol. Liq. 156 (2010) 76–81. https://doi.org/10.1016/j.molliq.2010.04.016.

[15] W. Meesorn, A. Shirole, D. Vanhecke, L.M. de Espinosa, C. Weder, A Simple and Versatile Strategy To Improve the Mechanical Properties of Polymer Nanocomposites with Cellulose Nanocrystals, Macromolecules. 50 (2017) 2364–2374. https://doi.org/10.1021/acs.macromol.6b02629.

[16] E. Kontturi, P. Laaksonen, M.B. Linder, Nonappa, A.H. Gröschel, O.J. Rojas, O. Ikkala, Advanced Materials through Assembly of Nanocelluloses, Adv. Mater. 30 (2018) 1–36. https://doi.org/10.1002/adma.201703779.

[17] H. Oguzlu, C. Danumah, Y. Boluk, The role of dilute and semi-dilute cellulose nanocrystal (CNC) suspensions on the rheology of carboxymethyl cellulose (CMC) solutions, Can. J. Chem. Eng. 94 (2016) 1841–1847. https://doi.org/10.1002/cjce.22597.

[18] S.P.S. Chundawat, G. Bellesia, N. Uppugundla, L. Da Costa Sousa, D. Gao, A.M. Cheh, U.P. Agarwal, C.M. Bianchetti, G.N. Phillips, P. Langan, V. Balan, S. Gnanakaran, B.E. Dale, Restructuring the crystalline cellulose hydrogen bond network enhances its depolymerization rate, J. Am. Chem. Soc. 133 (2011) 11163–11174. https://doi.org/10.1021/ja2011115.

[19] Y. Huang, C. Zhu, J. Yang, Y. Nie, C. Chen, D. Sun, Recent advances in bacterial cellulose, Cellulose. 21 (2014) 1–30. https://doi.org/10.1007/s10570-013-0088-z.

[20] K.R. Krishna Iyer, P. Neelakantan, T. Radhakrishnan, Birefringence of Native Cellulosic Fibres. I. Untreated Cotton and Ramie, J. Polym. Sci. 6 (1968) 1747–1758.

[21] C.L. McCormick, P.A. Callais, B.H. Hutchinson, Solution studies of cellulose in lithium chloride and N,N-dimethylacetamide, Macromolecules. 18 (1985) 2394–2401. https://doi.org/10.1021/ma00154a010.

[22] E.E. Ureña-Benavides, G. Ao, V.A. Davis, C.L. Kitchens, Rheology and Phase Behavior of Lyotropic Cellulose Nanocrystal Suspensions, Macromolecules. 44 (2011) 8990–8998. https://doi.org/10.1021/ma201649f.

[23] R.H. Marchessault, F.F. Morehead, N.M. Walter, Liquid Crystal Systems from Fibrillar Polysaccharides, Nature. 184 (1959) 632–633. https://doi.org/10.1038/184632a0.

[24] A.A. Hamza, H.I. Abd el-Kader, Optical Properties and Birefringence Phenomena in Fibers, Text. Res. J. 53 (1983) 205–209. https://doi.org/10.1177/004051758305300401.

[25] A. Mendoza-Galván, T. Tejeda-Galán, A. Domínguez-Gómez, R. Mauricio-

Sánchez, K. Järrendahl, H. Arwin, Linear Birefringent Films of Cellulose Nanocrystals Produced by Dip-Coating, Nanomaterials. 9 (2018) 45–57. https://doi.org/10.3390/nano9010045.

[26] K. Uetani, H. Koga, M. Nogi, Estimation of the Intrinsic Birefringence of Cellulose Using Bacterial Cellulose Nanofiber Films, ACS Macro Lett. 8 (2019) 250–254. https://doi.org/10.1021/acsmacrolett.9b00024.

[27] C. Hagiopol, Chemistry of modern papermaking, CRC, 2011.

[28] M.I. Tobler-Rohr, Handbook of sustainable textile production, 2011.

[29] J. Cai, L. Zhang, Unique gelation behavior of cellulose in NaOH/urea aqueous solution, Biomacromolecules. 7 (2006) 183–189. https://doi.org/10.1021/bm0505585.

[30] T. Budtova, P. Navard, Cellulose in NaOH–water based solvents: a review, Cellulose. 23 (2016) 5–55. https://doi.org/10.1007/s10570-015-0779-8.

[31] N. Lavoine, I. Desloges, J. Bras, Microfibrillated cellulose coatings as new release systems for active packaging, Carbohydr. Polym. 103 (2014) 528–537. https://doi.org/10.1016/j.carbpol.2013.12.035.

[32] K. Jedvert, T. Heinze, Cellulose modification and shaping - A review, J. Polym. Eng. 37 (2017) 845–860. https://doi.org/10.1515/polyeng-2016-0272.

[33] G. Rodionova, M. Lenes, Ø. Eriksen, Ø. Gregersen, Surface chemical modification of microfibrillated cellulose: Improvement of barrier properties for packaging applications, Cellulose. 18 (2011) 127–134. https://doi.org/10.1007/s10570-010-9474-y.

[34] D.B.G. Williams, J.M. Mason, C.J. Tristram, S.F.R. Hinkley, Cellulose as a Source of Water Dispersible Renewable Film-Forming Materials, Macromolecules. 48 (2015) 8497–8508. https://doi.org/10.1021/acs.macromol.5b02131.

[35] M. Shibakami, T. Nemoto, M. Sohma, Dependence of dissolution, dispersion, and aggregation characteristics of cationic polysaccharides made from euglenoid β-1,3-glucan on degree of substitution, Cellulose. 25 (2018) 2217–2234. https://doi.org/10.1007/s10570-018-1740-4.

[36] Y. Song, Y. Sun, X. Zhang, J. Zhou, L. Zhang, Homogeneous quaternization of cellulose in NaOH/Urea aqueous solutions as gene carriers, Biomacromolecules. 9 (2008) 2259–2264. https://doi.org/10.1021/bm800429a.

[37] J. Schaller, T. Heinze, Studies on the synthesis of 2,3-O-hydroxyalkyl ethers of cellulose, Macromol. Biosci. 5 (2005) 58–63. https://doi.org/10.1002/mabi.200400136.

[38] M. Gosecki, H. Setälä, T. Virtanen, A.J. Ryan, A facile method to control the phase behavior of hydroxypropyl cellulose, Carbohydr. Polym. 251 (2021) 1–7. https://doi.org/10.1016/j.carbpol.2020.117015.

[39] A.M. Bochek, Effect of hydrogen bonding on cellulose solubility in aqueous and nonaqueous solvents, Russ. J. Appl. Chem. 76 (2003) 1711–1719. https://doi.org/10.1023/B:RJAC.0000018669.88546.56.

[40] J.K. Fink, Reactive Polymers Fundamentals and Applications, Elsevier, 2013. https://doi.org/10.1016/C2012-0-02516-1.

[41] K. Xie, H. Tu, Z. Dou, D. Liu, K. Wu, Y. Liu, F. Chen, L. Zhang, Q. Fu, The effect of cellulose molecular weight on internal structure and properties of regenerated cellulose fibers as spun from the alkali/urea aqueous system, Polymer (Guildf). 215 (2021). https://doi.org/10.1016/j.polymer.2021.123379.

[42] R. Gallego, J.F. Arteaga, C. Valencia, J.M. Franco, Thickening properties of several NCO-functionalized cellulose derivatives in castor oil, Chem. Eng. Sci. 134 (2015) 260–268. https://doi.org/10.1016/j.ces.2015.05.007.

[43] F. Berthold, K. Gustafsson, E. Sjöholm, M. Lindström, An improved method for the determination of softwood kraft pulp molecular mass distributions, 11th Int. Syposium Wood Pulping Chem. 1 (2001) 363–366.

[44] M. Kaszuba, J. Corbett, F.M.N. Watson, A. Jones, High-concentration zeta potential measurements using light-scattering techniques, Philos. Trans. R. Soc. A Math. Phys. Eng. Sci. 368 (2010) 4439–4451. https://doi.org/10.1098/rsta.2010.0175.

[45] C.A. Schneider, W.S. Rasband, K.W. Eliceiri, NIH Image to ImageJ: 25 years of image analysis, Nat. Methods. 9 (2012) 671–675. https://doi.org/10.1038/nmeth.2089.

[46] J. Ilavsky, P.R. Jemian, Irena : tool suite for modeling and analysis of small-angle scattering , J. Appl. Crystallogr. 42 (2009) 347–353. https://doi.org/10.1107/s0021889809002222.

[47] O.O. Mykhaylyk, N.J. Warren, A.J. Parnell, G. Pfeifer, J. Laeuger, Applications of shear-induced polarized light imaging (SIPLI) technique for mechano-optical rheology of polymers and soft matter materials, J. Polym. Sci. Part B Polym. Phys. 54 (2016) 2151–2170. https://doi.org/10.1002/polb.24111.

[48] A. Paajanen, Y. Sonavane, D. Ignasiak, J.A. Ketoja, T. Maloney, S. Paavilainen, Atomistic molecular dynamics simulations on the interaction of TEMPO-oxidized cellulose nanofibrils in water, Cellulose. 23 (2016) 3449–3462. https://doi.org/10.1007/s10570-016-1076-x.

[49] J.F. Matthews, M. Bergenstråhle, G.T. Beckham, M.E. Himmel, M.R. Nimlos, J.W. Brady, M.F. Crowley, High-temperature behavior of cellulose i, J. Phys. Chem. B. 115 (2011) 2155–2166. https://doi.org/10.1021/jp1106839.

[50] S. Paavilainen, T. Róg, I. Vattulainen, Analysis of twisting of cellulose nanofibrils in atomistic molecular dynamics simulations, J. Phys. Chem. B. 115 (2011) 3747–3755. https://doi.org/10.1021/jp111459b.

[51] D.P. Oehme, M.S. Doblin, J. Wagner, A. Bacic, M.T. Downton, M.J. Gidley, Gaining insight into cell wall cellulose macrofibril organisation by simulating microfibril adsorption, Cellulose. 22 (2015) 3501–3520. https://doi.org/10.1007/s10570-015-0778-9.

[52] J. Ketoja, S. Paavilainen, J.L. McWhirter, T. Róg, J. Järvinen, I. Vattulainen, Mechanical properties of cellulose nanofibrils determined through atomistic molecular dynamics simulations, Nord. Pulp Pap. Res. J. 27 (2012) 282–286.

https://doi.org/10.3183/npprj-2012-27-02-p282-286.

[53] S. Peri, M. Nazmul Karim, R. Khare, Potential of mean force for separation of the repeating units in cellulose and hemicellulose, Carbohydr. Res. 346 (2011) 867–871. https://doi.org/10.1016/j.carres.2011.01.008.

[54] S. Plimpton, Fast parallel algorithms for short-range molecular dynamics, J. Comput. Phys. 117 (1995) 1–19. https://doi.org/10.1006/jcph.1995.1039.

[55] O. Guvench, S.N. Greenr, G. Kamath, J.W. Brady, R.M. Venable, R.W. Pastor, A.D. Mackerell, Additive empirical force field for hexopyranose monosaccharides, J. Comput. Chem. 29 (2008) 2543–2564. https://doi.org/10.1002/jcc.21004.

[56] O. Guvench, E. Hatcher, R.M. Venable, R.W. Pastor, A.D. Mackerell, CHARMM Additive All-Atom Force Field for Glycosidic Linkages between Hexopyranoses, (2009) 2353–2370.

[57] K. Vanommeslaeghe, E. Hatcher, C. Acharya, S. Kundu, S. Zhong, J. Shim, E. Darian, O. Guvench, P. Lopes, I. Vorobyov, A.D. Mackerell, CHARMM general force field: A force field for drug-like molecules compatible with the CHARMM all-atom additive biological force fields, J. Comput. Chem. 31 (2010) 671–690. https://doi.org/10.1002/jcc.21367.

[58] S. Donets, J.U. Sommer, Molecular Dynamics Simulations of Strain-Induced Phase Transition of Poly(ethylene oxide) in Water, J. Phys. Chem. B. 122 (2018) 392–397. https://doi.org/10.1021/acs.jpcb.7b10793.

[59] A. Luzar, D. Chandler, Effect of Environment on Hydrogen Bond Dynamics in Liquid Water, (1996).

[60] W. Humphrey, A. Dalke, K. Schulten, VMD : Visual Molecular Dynamics, 7855 (1996) 33–38.

[61] Dassault Systèmes BOVIA, (2014).

[62] S.R. Varanasi, O.A. Guskova, A. John, J.U. Sommer, Water around fullerene shape amphiphiles: A molecular dynamics simulation study of hydrophobic hydration, J. Chem. Phys. 142 (2015). https://doi.org/10.1063/1.4922322.

[63] L.M. Zhang, New water-soluble cellulosic polymers: A review, Macromol. Mater. Eng. 286 (2001) 267–275. https://doi.org/10.1002/1439-2054(20010501)286:5<267::AID-MAME267>3.0.CO;2-3.

[64] M.H. Godinho, D.G. Gray, P. Pieranski, Revisiting (hydroxypropyl) cellulose (HPC)/water liquid crystalline system, Liq. Cryst. 44 (2017) 2108–2120. https://doi.org/10.1080/02678292.2017.1325018.

[65] P. Choi, T.A. Kavassalis, A. Rudin, Estimation of Hansen Solubility Parameters for (Hydroxyethyl)- and (Hydroxypropyl)cellulose through Molecular Simulation, Ind. Eng. Chem. Res. 33 (1994) 3154–3159. https://doi.org/10.1021/ie00036a034.

[66] J. Brady, T. Dürig, P.I. Lee, J.-X. Li, Polymer Properties and Characterization, in: Dev. Solid Oral Dos. Forms, Second Edi, Elsevier, Boston, 2017: pp. 181–223. https://doi.org/10.1016/B978-0-12-802447-8.00007-8.

[67] S. Eyley, W. Thielemans, Surface modification of cellulose nanocrystals, Nanoscale. 6 (2014) 7764–7779. https://doi.org/10.1039/c4nr01756k.

[68] M. Kazharska, Y. Ding, M. Arif, F. Jiang, Y. Cong, H. Wang, C. Zhao, X. Liu, Z. Chi, C. Liu, Cellulose nanocrystals derived from Enteromorpha prolifera and their use in developing bionanocomposite films with water-soluble polysaccharides extracted from E. prolifera, Int. J. Biol. Macromol. 134 (2019) 390–396. https://doi.org/10.1016/j.ijbiomac.2019.05.058.

[69] I. Shahabi-Ghahfarrokhi, F. Khodaiyan, M. Mousavi, H. Yousefi, Preparation and characterization of nanocellulose from beer industrial residues using acid hydrolysis/ultrasound, Fibers Polym. 16 (2015) 529–536. https://doi.org/10.1007/s12221-015-0529-4.

[70] B. Pereira, V. Arantes, Nanocelluloses From Sugarcane Biomass, in: Adv. Sugarcane Biorefinery, Elsevier, 2018: pp. 179–196. https://doi.org/10.1016/B978-0-12-804534-3.00009-4.

[71] M. Le Gars, L. Douard, N. Belgacem, J. Bras, Cellulose Nanocrystals: From Classical Hydrolysis to the Use of Deep Eutectic Solvents, in: Nanosystems, IntechOpen, 2019. https://doi.org/10.5772/intechopen.89878.

[72] M.A. Smirnov, M.P. Sokolova, D.A. Tolmachev, V.K. Vorobiov, I.A. Kasatkin, N.N. Smirnov, A. V. Klaving, N. V. Bobrova, N. V. Lukasheva, A. V. Yakimansky, Green method for preparation of cellulose nanocrystals using deep eutectic solvent, Cellulose. 27 (2020) 4305–4317. https://doi.org/10.1007/s10570-020-03100-1.

[73] D.A. Gopakumar, Y.B. Pottathara, K.T. Sabu, H.P.S. Abdul Khalil, Y. Grohens, S. Thomas, Nanocellulose-based aerogels for industrial applications, in: Ind. Appl. Nanomater., Elsevier, 2019: pp. 403–421. https://doi.org/10.1016/B978-0-12-815749-7.00014-1.

[74] Y. Mao, K. Liu, C. Zhan, L. Geng, B. Chu, B.S. Hsiao, Characterization of Nanocellulose Using Small-Angle Neutron, X-ray, and Dynamic Light Scattering Techniques, J. Phys. Chem. B. 121 (2017) 1340–1351. https://doi.org/10.1021/acs.jpcb.6b11425.

[75] R.E. Cameron, J. Crawshaw, G.R. Mant, W. Bras, Simultaneous SAXS and WAXS investigations of changes in native cellulose fiber microstructure on swelling in aqueous sodium hydroxide, J. Appl. Polym. Sci. 83 (2002) 1209–1218. https://doi.org/10.1002/app.2287.

[76] K. Leppänen, K. Pirkkalainen, P. Penttilä, J. Sievänen, N. Kotelnikova, R. Serimaa, Small-angle x-ray scattering study on the structure of microcrystalline and nanofibrillated cellulose, J. Phys. Conf. Ser. 247 (2010) 1–11. https://doi.org/10.1088/1742-6596/247/1/012030.

[77] F. Horkay, A.M. Hecht, E. Geissler, Fine structure of polymer networks as revealed by solvent swelling, Macromolecules. 31 (1998) 8851–8856. https://doi.org/10.1021/ma971606j.

[78] E. Benigar, I. Dogsa, D. Stopar, A. Jamnik, I.K. Cigić, M. Tomšič, Structure and dynamics of a polysaccharide matrix: Aqueous solutions of bacterial levan, Langmuir. 30 (2014) 4172–4182. https://doi.org/10.1021/la500830j.

[79] B. Hammouda, D. Ho, S. Kline, SANS from poly(ethylene oxide)/water systems, Macromolecules. 35 (2002) 8578–8585. https://doi.org/10.1021/ma011657n.

[80] M. Doi, The Theory of Polymer Dynamics, J. Nonnewton. Fluid Mech. 25 (1987) 385–386. https://doi.org/10.1016/0377-0257(87)85036-x.

[81] B. Hammouda, D.L. Ho, S. Kline, Insight into clustering in poly(ethylene oxide) solutions, Macromolecules. 37 (2004) 6932–6937. https://doi.org/10.1021/ma049623d.

[82] I. Dogsa, M. Tomšič, J. Orehek, E. Benigar, A. Jamnik, D. Stopar, Amorphous supramolecular structure of carboxymethyl cellulose in aqueous solution at different pH values as determined by rheology, small angle X-ray and light scattering, Carbohydr. Polym. 111 (2014) 492–504. https://doi.org/10.1016/j.carbpol.2014.04.020.

[83] B. Hammouda, SANS from homogeneous polymer mixtures: A unified overview, Polym. Charact. 106 (1993) 87–133. https://doi.org/10.1007/BFb0025862.

[84] I. Dogsa, J. Cerar, A. Jamnik, M. Tomšič, Supramolecular structure of methyl cellulose and lambda- and kappa-carrageenan in water: SAXS study using the string-of-beads model, Carbohydr. Polym. 172 (2017) 184–196. https://doi.org/10.1016/j.carbpol.2017.04.048.

[85] E. Benigar, A. Zupančič Valant, I. Dogsa, S. Sretenovic, D. Stopar, A. Jamnik, M. Tomšič, Structure and Dynamics of a Model Polymer Mixture Mimicking a Levan-Based Bacterial Biofilm of Bacillus subtilis, Langmuir. 32 (2016) 8182–8194. https://doi.org/10.1021/acs.langmuir.6b02041.

[86] W. Van De Sande, A. Persoons, The size and shape of macromolecular structures: Determination of the radius, the length, and the persistence length of rodlike micelles of dodecyldimethylammonium chloride and bromide, J. Phys. Chem. 89 (1985) 404–406. https://doi.org/10.1021/j100249a007.

[87] S. Park, J.O. Baker, M.E. Himmel, P.A. Parilla, D.K. Johnson, Cellulose crystallinity index: measurement techniques and their impact on interpreting cellulase performance, Biotechnol. Biofuels. 3 (2010) 1–10. https://doi.org/10.1186/1754-6834-3-10.

[88] J. Blackwell, D. Kurz, M.-Y. Su, D.M. Lee, X-ray Studies of the Structure of Cellulose Complexes, in: Struct. Cellul., American Chemical Society, 1987: pp. 199–213. https://doi.org/10.1021/bk-1987-0340.ch012.

[89] M. Saito, Wormlike Chain Parameters of Cellulose and Cellulose Derivatives, Polym. J. 15 (1983) 213–223. https://doi.org/10.1295/polymj.15.213.

[90] M. Moan, C. Wolff, Study of the conformational rigidity of polyelectrolytes by elastic neutron scattering: 1. Carboxymethylcelluloses in the intermediate momentum range, Polymer (Guildf). 16 (1975) 776–780. https://doi.org/10.1016/0032-3861(75)90105-6.

[91] R.M. Davis, Analysis of Dilute Solutions of (Carboxymethyl) cellulose with the Electrostatic Wormlike Chain Theory, Macromolecules. 24 (1991) 1149–1155.

https://doi.org/10.1021/ma00005a027.

[92] G.J. Gerwig, J. Van Albert Kuik, B.R. Leeflang, J.P. Kamerling, J.F.G. Vliegenthart, C.D. Karr, E.L. Jarroll, The Giardia intestinal filamentous cyst wall contains a novel β(1-3)-N-acetyl-D-galactosamine polymer: A structural and conformational study, Glycobiology. 12 (2002) 499–505. https://doi.org/10.1093/glycob/cwf059.

[93] S.J. Picken, D.J. Sikkema, H. Boerstoel, T.J. Dingemans, S. van der Zwaag, Liquid crystal main-chain polymers for high-performance fibre applications, Liq. Cryst. 38 (2011) 1591–1605. https://doi.org/10.1080/02678292.2011.624367.

[94] M. Yamaguchi, M.E.A. Manaf, K. Songsurang, S. Nobukawa, Material design of retardation films with extraordinary wavelength dispersion of orientation birefringence: A review, Cellulose. 19 (2012) 601–613. https://doi.org/10.1007/s10570-012-9660-1.

[95] E.D. Cranston, D.G. Gray, Birefringence in spin-coated films containing cellulose nanocrystals, Colloids Surfaces A Physicochem. Eng. Asp. 325 (2008) 44–51. https://doi.org/10.1016/j.colsurfa.2008.04.042.

[96] O.O. Mykhaylyk, Time-resolved polarized light imaging of sheared materials: Application to polymer crystallization, Soft Matter. 6 (2010) 4430–4440. https://doi.org/10.1039/c0sm00332h.

[97] M. Born, E. Wolf, A.B. Bhatia, P.C. Clemmow, D. Gabor, A.R. Stokes, A.M. Taylor, P.A. Wayman, W.L. Wilcock, Principles of Optics, 7th ed., Cambridge University Press, 1999. https://doi.org/10.1017/CBO9781139644181.

[98] K. Wulf, Polymer melt rheology and flow birefringence. Von H. Janeschitz-Kriegl. Band 6 der Reihe Polymers/Properties and Applications. ISBN 3-540-11928-0. Berlin/Heildelberg/New York:Springer-Verlag 1983. XV, 524 S., geb. DM 98.–, Acta Polym. 36 (1985) 296–297. https://doi.org/10.1002/actp.1985.010360522.

[99] N.J. Warren, M.J. Derry, O.O. Mykhaylyk, J.R. Lovett, L.P.D. Ratcliffe, V. Ladmiral, A. Blanazs, L.A. Fielding, S.P. Armes, Critical Dependence of Molecular Weight on Thermoresponsive Behavior of Diblock Copolymer Worm Gels in Aqueous Solution, Macromolecules. 51 (2018) 8357–8371. https://doi.org/10.1021/acs.macromol.8b01617.

[100] M.L. Coughlin, L. Liberman, S.P. Ertem, J. Edmund, F.S. Bates, T.P. Lodge, Methyl cellulose solutions and gels: fibril formation and gelation properties, Prog. Polym. Sci. 112 (2021) 101324. https://doi.org/10.1016/j.progpolymsci.2020.101324.

[101] Y. Shen, H. Orelma, A. Sneck, K. Kataja, J. Salmela, P. Qvintus, A. Suurnäkki, A. Harlin, High velocity dry spinning of nanofibrillated cellulose (CNF) filaments on an adhesion controlled surface with low friction, Cellulose. 23 (2016) 3393–3398. https://doi.org/10.1007/s10570-016-1044-5.

[102] Y. Shen, A. Harlin, J. Salmela, Method for producing high tensile strength nanofiber yarn, WO 2016/102782 A1, 2016. https://worldwide.espacenet.com/publicationDetails/biblio?CC=WO&NR=2016102782A1&KC=A1&FT=D#.